CELL-FREE STUDIES OF CATALYTIC DNA CLEAVAGE BY RUTHENIUM POLYPYRIDYL COMPLEXES (RPCS) CONTAINING REDOX-ACTIVE INTERCALATING LIGANDS, ENANTIOMERIC SEPARATION AND SEMI-PREP SCALE PURIFICATION OF RPCS

by

CYNTHIA ANN GRIFFITH

Presented to the Faculty of the Graduate School of

The University of Texas at Arlington in Partial Fulfillment

of the Requirements

for the Degree of

DOCTOR OF PHILOSOPHY

THE UNIVERSITY OF TEXAS AT ARLINGTON

August 2018

Acknowledgements

I would like to acknowledge my deepest gratitude to my advisor Dr. Frederick MacDonnell. My desire to achieve a PhD and the opportunity to discover my love for chemistry and research would never have been possible without the opportunity given to me by my greatest influence, Dr. Frederick MacDonnell. He took a chance on me and supported me against all odds so that I could achieve my goals in higher education. In addition to being an advisor, he served as mentor, provided guidance not only in research but in life as well. He provided a working environment that allowed me to grow exponentially. Through his guidance I learned how to see past my own circumstances and maintain the necessary focus to complete my research and maintain a work life balance. In addition to Dr. MacDonnell, I would like to thank my committee members, Dr. Kayunta Johonson-Winters, Dr. Brad Pierce, and Dr. Daniel Armstrong. They too contributed to my success and growth as a researcher and student. Furthermore all of committee members including my academic advisors, Dr. Kroll and Dr. Foss have shown me great patience and inspiration in the field of chemistry. There are no words to describe my gratitude and appreciation for their continued support.

I would like to also thank all of my lab mates over the years for their endless support and encouragement. A special thanks goes to Dr. Choyce Weatherly and Dr. Nagham Alatrash. I am certain that without their faith in me, the rigor of completing my research would have been unbearable. Not only did they support and challenge me but they helped me greatly in the lab as well. My work could not have progressed as rapidly as it did without their help.

In addition, I would like to thank the dedication and support of the faculty and staff of the Chemistry and Biochemistry Department including, Dr. Bill Cleaver, Dr. Heidi Conrad, Dr. Roy McDougald, Dr. Brian Edwards, Debbie Cooke, Natalie Croy, Beth Klimek, and Jill Howard, for their friendship and assistance during these past years. They are all dedicated to the highest standards and success of all the students in the department. Due to their deepest desire to construct and maintain a department dedicated to the success of the students in academia as well as in industry, I have been able to achieve my goals towards earning a PhD in Chemistry at the age of 45. I have been given a second chance at life because of the dedication and support I received from family, friends, and this university. Finally, I would like to acknowledge the support and sacrifice my family has given and endured throughout this rigorous process. I would like to start with my children Elizabeth, Tanner, Anthony, Jessica, Michael, and Samantha Hennegan. I would also like to thank my father and stepmother, John and Kathy Griffith. Last but not least I owe my greatest acknowledgment to my best friends, Matthew Noble, Rachel Garcia, Andy Seal, Kate Nguyen, and Diego Lopez. . Had it not been for their continued support and faith in me I would not have been able to complete my research or this degree.

July 18, 2018

Abstract

CELL-FREE STUDIES OF CATALYTIC DNA CLEAVAGE BY RUTHENIUM POLYPYRIDYL COMPLEXES (RPCS) CONTAINING REDOX-ACTIVE INTERCALATING LIGANDS, ENANTIOMERIC SEPARATION AND SEMI-PREP SCALE PURIFICATION OF RPCS

Cynthia Griffith, PhD

The University of Texas at Arlington, 2018

Supervising Professor: Frederick M. MacDonnell

Herein, we report the ruthenium (II) polypyridyl complexes (RPCs), $[(phen)_2Ru(tatpp)]^{2+}$ (**3**$^{2+}$) and $[(phen)_2Ru(tatpp)Ru(phen)_2]^{4+}$ (**4**$^{4+}$) are shown to cleave DNA in cell-free studies in the presence of a mild reducing agent, i.e. glutathione (GSH), in a manner that is enhanced upon lowering the $[O_2]$. Reactive oxygen species (ROS) are involved in the cleavage process as hydroxy radical scavengers attenuate the cleavage activity. Cleavage experiments in the presence of superoxide dismutase (SOD) and catalase reveal a central role for H_2O_2 as the immediate precursor for hydroxy radicals. A mechanism is proposed which explains the inverse $[O_2]$dependence and ROS data and involves redox cycling between three DNA-bound redox isomers of **3**$^{2+}$ or **4**$^{4+}$. Cultured non-small cell lung cancer cells (H358) are sensitive to **3**$^{2+}$ and **4**$^{4+}$ with IC_{50} values of 13 and 15 μM, respectively, and xenograft H358 tumors in nude mice show substantial (~ 80%) regression relative to untreated tumors when the mice are treated with enantiopure versions of **3**$^{2+}$ and **4**$^{4+}$.(Yadav et.al. *Mol Cancer Res*, **2013**, *12*, 643) Fluorescent

microscopy of H358 cells treated with 15 μM $\mathbf{4}^{4+}$ reveals enhanced intracellular ROS production in as little as 2 h post treatment. Detection of phosphorylated ATM via immunofluorescence within 2 h of treatment with $\mathbf{4}^{4+}$ reveals initiation of the DNA damage repair machinery due to the ROS insult and DNA double strand breaks (DSBs) in the nuclei of H358 cells and is confirmed using the γH2AX assay. The cell data for $\mathbf{3}^{2+}$ is less clear but DNA

damage occurs. Notably, cells treated with $[Ru(diphenylphen)_3]^{2+}$ (IC_{50} 1.7 μM) show no extra ROS production and no DNA damage by either the pATM or γH2AX even after 22 h. The enhanced DNA cleavage under low $[O_2]$(4 μM) seen in in cell-free cleavage assays of $\mathbf{3}^{2+}$ and $\mathbf{4}^{4+}$ is only partially reflected in the cytotoxicity of $\mathbf{3}^{2+}$ and $\mathbf{4}^{4+}$ in H358, HCC2998, HOP-62 and Hs766t under hypoxia (1.1 % O_2) relative to normoxia (18% O_2). Cells treated with RPC $\mathbf{3}^{2+}$ show up to a two-fold enhancement in the IC_{50} under hypoxia whereas cells treated with RPC $\mathbf{4}^{4+}$ gave the same IC_{50} whether under hypoxia or normoxia.

We also report herein method development for semi-preparative scale HPLC enantiomeric separation and purification of the ruthenium (II) polypyridyl complex $[Ru(phen)_2$ phendione$]^{2+}$.The results of the retention factor vs. methanol/acetonitrile ratio plot indicated different interactions take place at different polar organic solvent compositions. Interestingly, the results of the selectivity, retention factor, and resolution vs. Methanol/ acetonitrile ratio plot showed no significant change in selectivity as the retention factor and resolution increased. This allowed the focus for semi-prep scale method optimization to be on retention time.

Finally, we report the method development and optimization of six Ru(II) dyads derived from thiophene (1T) and oligothiophenes (4T) for chiral separation and enantiomeric purification in polar organic mode using HPLC. The results of the retention factor vs. methanol/acetonitrile ratio plot indicated different interactions take place at different polar organic solvent compositions. Although selectivity and resolution remained relatively constant the retention factors increased with increasing amounts of methanol. However, the retention factor increases significantly with increasing retention times, allowing the focus of optimization to be on shortening the retention while maintaining[GCA1] resolution. These results are important for later use in semi-preparative enantiomeric purification by allowing the focus to be on optimal retention time.

Table of Contents

Chapter 1

INTRODUCTION TO CANCER AND CHEMOPTHERAPY

1.1 Perspective

Cancer is a group of approximately 100 diseases. Uncontrolled growth of abnormal (cancerous) cells and the ability of these cells to migrate from the original site of origin to a different organ system site (metastasis) are the two main characteristics of cancer. If metastasis occurs cancer may result in death. According to the National Vital Statistics (NVSS) by the Centers for Disease Control (CDC) on December 20, 2013, the top ten leading causes of death were reported for 2010[1] with 75% of the top ten causes accounting for all deaths in the United States. The report showed a total number of deaths at 2,596,993 at a rate of 821.5 deaths per 100,000 population with a life expectancy of 78.8 years. The leading cause of death was heart disease with 611,105 deaths. The second with 584,881 deaths was caused by malignant neoplasms (cancer or malignant tumor). All other causes were at or less than 149,205 deaths per remaining cause. Given the mortality rate of cancer much effort has been invested for drug development to treat cancer with minimal side effects.

Chemotherapy is the systemic treatment of cancer with the use of medicinal drugs. A chemotherapeutic agent is a general term used to identify drugs or molecular compounds used to treat cancer.[2] The majority of these agents disrupt rapidly dividing cells that leads to cellular death or apoptosis.[3] Chemotherapeutic agents can be classified into the following groups, alkylating agents, anti-tumor antibiotics, antimetabolites, topoisomerase inhibitors, mitotic

inhibitors, corticosteroids and miscellaneous chemotherapy drugs. These classifications are based on factors such as chemical structure, function and their relationship to other drugs. Furthermore, chemotherapeutic agents are not limited to any one group or classification.[4]

Transition metal based chemotherapeutic drugs have been used to treat cancer since the late 1970's. More specific, cisplatin was approved for clinical use in 1978. However, platinum-based chemotherapeutics have limitations in low solubility, toxic side effects, and tumor resistance.[5,6] Therefore, researchers have investigated other metal based chemotherapeutics that are able to overcome the side effects and potential resistance as seen with cisplatin and its derivatives. Considerations for alternative heavy metal complexes are the inherent toxicity of the metal complex(s) and the body's ability to remove or prevent accumulation of metal ions.[7]

Ruthenium polypyridyl complexes RPCs have become up and coming drugs of interested due to their similar substitution kinetics of platinum based drugs[8] and from extensive work by the Dwyer group showing these complexes do not accumulate in the body.[9-11] In addition, RPC's show different biological activity than cisplatin and its derivatives.[10] This is significant as possible alternative treatments for tumors that develop resistance to cisplatin and its analogues.[12]

Due to the robust nature, distinctive electrochemical and photophysical characteristics of ruthenium(II) polypyridyl complexes a wide variety of RPCs have been synthesized and investigated for a multitude of applications ranging

from energy to medicinal uses. Many RPCs are known to have specific interactions with DNA and have been widely used for cellular imaging and therapeutics, as they are known to have specific interactions with DNA.[13-15] In addition to medicinal investigations and uses, ruthenium(II) complexes are effective catalysts for organic synthesis and dye sensitizers for solar cells.[16-19] Ruthenium(II) polypyridyl are complexes that exhibit axial chirality and the right- and left-handed configurations of the octahedral complexes are referred to as Δ- and Λ-enantiomers respectively. It is known the enantiomers of ruthenium(II) complexes exhibit very different biological activities when used as inhibitors of enzyme activity, DNA intercalating agents, and stabilizers of G-Quadruplex DNA.[20-22] When RPCs are used as a catalyst, enantiomers of ruthenium(II) complexes dramatically influence the stereochemistry of chiral products.[23] Therefore, the need for analytical methods by which ruthenium(II) polypyridyl complex enantiomers can be separated, evaluated, and purified cannot be overstated.

1.2 Scope of Thesis

This thesis describes our investigation of the chemical mechanism of cationic, RPCs ability to cleave DNA in cellular and non-cellular environments. In addition to this, method development for analytical and semi-preparative scale enantiomeric purification of the RPC's developed by the MacDonnell group and the McFarland group was investigated and optimized.

Chapter 2: Cellular and cell-free studies of catalytic DNA cleavage by ruthenium polypyridyl complexes containing redox-active intercalating ligands, a published work (2017), discusses the investigation of the chemical mechanism of RPCs from the MacDonnell group to cleave DNA. Cellular investigations in this work was done by Dr. Dayoub and Ali Mohammed. Cell free work was done by Cynthia Griffith. The discovery and electrochemistry of RPCs investigated was the work of Thamara Jaranatne. Nagham Alatrash contributed to the synthesis of RPCs from the MacDonnell. Kenneth Abayan contributed to hypoxia studies in cell free conditions. Zach Breitbach contributed to initial screening of DNA scission products.

Chapter 3: RPC enantiomeric separation and semi-prep scale purification by HPLC is discussed in chapter 3. In this work we investigated method development of semi preparative scale enantiomeric separation and purification of [Ru(phen)2 phendione]$^{2+}$ to be used for a symmetric synthesis of desire RPCs. RPC enantiomeric separation and semi-prep scale purification of Ru(I) and (II) dyads in a collaborative work with the McFarland Group with the University of North Carolina at Greensboro. In this work we investigate the method

development of five Ru(II) and one Ru(I) dyads to optimize methods for semi preparative scale enantiomeric purification.

Chapter 2

CELLULAR AND CELL-FREE STUDIES OF CATALYTIC DNA CLEAVAGE BY RUTHENIUM POLYPYRIDYL COMPLEXES CONTAINING REDOX-ACTIVE INTERCALATING LIGANDS

Published 8-2017

Cynthia Griffith , Adam S. Dayoub , Thamara Jaranatne , Nagham Alatrash , Ali Mohamedi , Kenneth Abayan , Zachary S. Breitbach , Daniel W. Armstrong and Frederick M. MacDonnell

2.1 Introduction

The use of transition-metal complexes in medicine has enjoyed extensive attention given the tremendous success of cisplatin (cis-$Pt(NH_3)_2Cl_2$) as a chemotherapeutic agent and the ability of many metal complexes to interact with and damage cellular structures, particularly DNA.[24-26] While research in metallopharmaceuticals continues to focus on platinum complexes, ruthenium complexes with labile chloride ligands are also explored as their substitution kinetics are similar to that of platinum. The promise of such compounds being their potential applicability to a wider-range of tumors and less severe toxicity relative to cisplatin. The anti-tumor agents NAMI-A (Imidazolium [trans-imidazoledimethylsulfoxide-tetrachlororuthenate(III), KP1019 (Indazolium [trans-tetrachlorobis(1H-indazole) ruthenate(III)]), RDC11 ([cis-bis(acetonitrile)-1,10-phenanthroline-2-phenylpyridineruthenium(II)] hexafluorophosphate),[27] and ruthenium-aryl-X complexes,[28] such as RAPTA-C,[29] all contain labile ligands and the loss of these ligands and subsequent binding of the ruthenium to biological

substrates is implicated in their biological activity. As many of these complexes contain Ru(III) ions, activation by bioreduction to Ru(II) is known to be essential to their mode of action.[30, 31] NAMI-A and KP1019 are reported to have advanced to Stage I and II clinical trials.[32-37]

Ruthenium polypyridyl complexes (RPCs), which we will constrain to Ru(II) complexes that are coordinatively saturated with polypyridyl ligands, constitute a fundamentally different class of metallo-drugs than those with labile ligands. RPCs have enjoyed the most attention in chemotherapeutic applications as photodynamic therapy (PDT) agents, some of which show demonstrable tumor reduction in vivo.[38-40] Photoexcitation of the RPC in the metal to ligand charge transfer (MLCT) region generates long-lived triplet species which can activate O_2 to form ROS,[41-47] directly oxidize DNA,[48,49] or induce ligand loss,[50-53] such that the released ligand or resulting complex is damaging to the DNA. Because the metal ion in a RPC is coordinatively saturated and substitutionally inert, it is generally unable to directly form bonds with biological targets, unless activated with light, which is in contrast to complexes such as NAMI-A, RAPTA-C, and KP1019. That said, RPCs do show some interesting biological activity even without light activation.

The homoleptic complexes, such as the trisphenanthroline complex ($\mathbf{1}^{2+}$) and the trisbipyridine complex shown in Figure 1, were extensively studied by the groups of Dwyer and Shulman in the 1950's and 1960's.[54] RPCs $\mathbf{1}^{2+}$ and $\mathbf{2}^{2+}$ are modestly cytotoxic (IC_{50}'s between 10^{-3} and 10^{-4} M) with enhanced cytotoxicity generally observed by increasing the lipophilicity of the complex.[55,56] The 3,4,7,8-

tetramethyl-1,10-phenanthroline derivative of $\mathbf{1}^{2+}$ was shown to inhibit the growth of dispersed tumor cells (Land Shultz ascites) in mice.[57] Early studies in which radiolabeled $[^{106}Ru(phen)_3]^{2+}$ was injected intraperitoneally into mice and rats showed that the intact complex cation was the bioactive unit, it was not metabolized in vivo, it did not accumulate in any organ in amounts greater than blood, and nearly all the complex was recovered in the urine.[58]

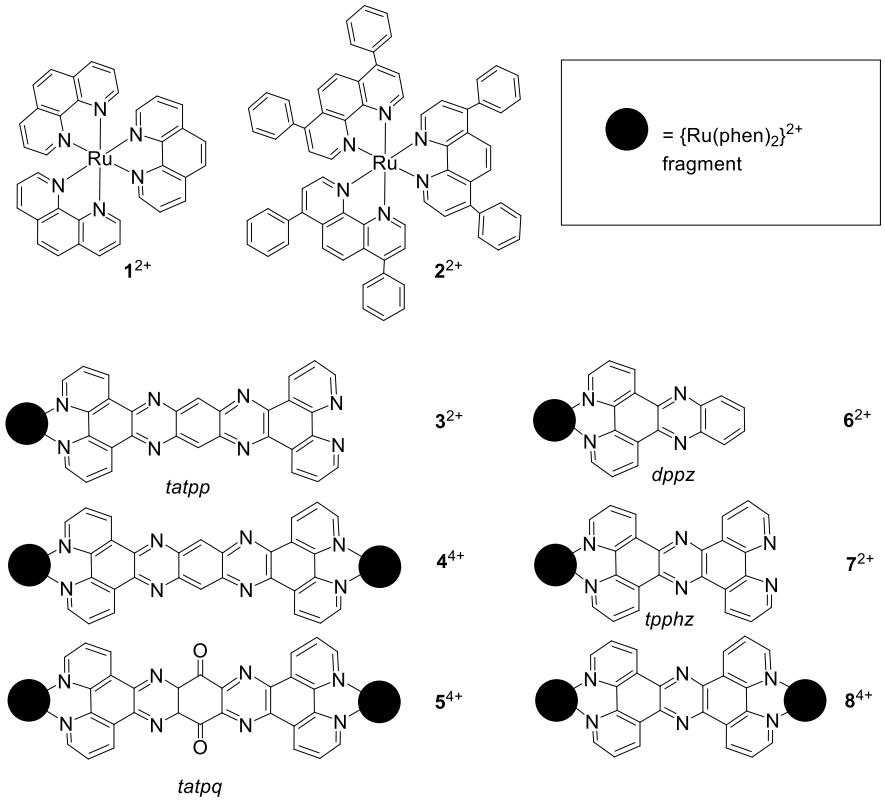

Figure 1 Chemical structures of RPCs and reference numbering scheme. All of these cations are soluble in water as the chloride salts.

More recently, the DNA-binding and molecular-light switch behavior of $[Ru(phen)_2(dppz)]^{2+}$ ($\mathbf{6}^{2+}$)[59] and $[Ru(phen)_2(tpphz)]^{2+}$ ($\mathbf{7}^{2+}$)[60,61] has led to a resurgence in this area, with numerous studies of their uses as biological probes[13,62-66] and the inherent (non-light activated) cytotoxicity of RPCs.[56,61,65,67-75] Because of the tendency of RPCs to bind DNA, it is often assumed that this is the biological target,[76-78] although recent data reveal that other cellular organelles are sometimes targeted, including the mitochondria,[67,73,75,79-84] endoplasmic reticulum,[64] ribosomes[85] and cell membrane.[12,86-90] It is not known how these RPCs act on the molecular targets but given their chemical inertness, it is postulated they non-covalently bind at specific sites disrupting important cellular processes.

Given the extensive attention of RPCs binding to DNA, it is somewhat surprising that very few cause observable damage unless they are activated by an external factor, such a light irradiation.[40,41,87,89,91,92] We have shown that the two ruthenium(II)-tatpp complexes, $\mathbf{3}^{2+}$ and $\mathbf{4}^{4+}$ (shown in Figure 1) are effective DNA cleaving agents upon in situ reduction by common biological reducing agents, such as glutathione.[12,90] This is not a light activated process and thus these complexes have potential as systemic chemotherapeutics which can seek out and kill micro-metastases whose presence and location are unknown. In contrast, PDT requires knowing the location of the metastases for effective treatment, although there is now evidence that such treatments can sometimes boost the systemic immune response.[93] The DNA cleavage activity of $\mathbf{3}^{2+}$ and $\mathbf{4}^{4+}$ in cell-free assays is enhanced under low oxygen conditions which is both

unusual and potentially beneficial as many tumors possess hypoxic regions.[12,90] Their anti-tumor efficacy has been demonstrated in mouse models in which nude mice bearing xenograph H358 tumors in their thighs showed an ~83% regression of tumor growth and more than doubling survival time upon intraperitoneal treatment with enantiopure Δ-**3**$^{2+}$ and ΔΔ-**4**$^{4+}$.[12] While direct proof was lacking, we postulated that the in vivo activity was also due to DNA damage.

In this paper, we demonstrate that these two RPCs catalytically induce DNA single-starnd breaks (SSBs) by activation of O_2 through a multi-stage redox-cycling mechanism which generates not only superoxide, but the more potent reactive oxygen species (ROS), H_2O_2. Significantly, at lower [O_2] there is a greater build-up of a doubly-reduced versions of **3**$^{2+}$ and **4**$^{4+}$, which are competent for direct H_2O_2 formation upon reaction with O_2. Thus a lower [O_2] favors enhanced catalytic formation of H_2O_2 over superoxide, the former being more effectively converted into the highly toxic hydroxyl radical species. Significantly, we can show that ROS is generated in the nuclei of cultured human non-small cell lung carcinoma (NSCLC) cells (H358) within 2 h of treatment with **3**$^{2+}$ or **4**$^{4+}$. Moreover, multiple DNA double strand breaks (DSBs) are also detected using immunofluorescent techniques to reveal the presence of pATM, an early marker of ROS induced DNA DSB damage, and γH2AX, a downstream marker of DNA DSBs. For cells treated with **4**$^{4+}$ this is evident within 2 hours of treatment whereas for **3**$^{2+}$, the induction period is considerably longer, on the order of 8 h. To the best of our knowledge, this is the first time that the cell-free

DNA cleavage activity of a ruthenium-based drug has been directly correlated with nuclear DNA damage in live human cancer cells.

2.2 EXPERIMENTAL

2.2.1 Chemicals

RPCs [**1**] Cl_2,[94] [**2**] Cl_2,[95] [**3**] Cl_2,[96] [**4**] Cl_4,[97] [**5**] Cl_4,[97] [**6**] Cl_2, [**7**] Cl_2,[98,99] [**8**] Cl_4,[99] were prepared as described in the literature and were used as the chloride salts. All RPCs were used as racemates or diasterotopic mixtures. Furfural standard was purchased from Sigma Aldrich. 5-Methylene furanone (5MF) was synthesized according to literature[100] using the modified procedure described below. The intermediate 3,5-di-O-p-toluoyl-2-deoxy-D-ribono-1,4-lactone was converted to 5-MF using Schlenk line techniques under a N_2 atmosphere. The final product structure was confirmed using GCMS for which the MS pattern matched that reported for 5-MF.[101] All reagents for the 5-MF synthesis were purchased from Sigma Aldrich.

2.2.2 In vitro DNA cleavage assays

All chemicals for buffers and related in vitro DNA experiments were purchased commercially and used without further purification unless otherwise noted. Millipore water was used for all buffers and reactions that required water. All plasmid DNA (pUC18 and pUC19) and DNA ladders were purchased from Bayou Biolabs. Chemicals needed for the DNA electrophoresis assay, ethidium bromide, GSH, trizma base, mono and dibasic phosphates,

ethylenediaminetetraacetic acid (EDTA) and agarose were purchased from Sigma Aldrich. Chemicals for the T4 ligase assay, T4 DNA ligase high concentration (HC), T4 DNA ligase 10X buffer, acetylated bovine serum albumin, EcoRI, and buffer HC 10X buffer were purchased from Promega.

DNA cleavage experiments were conducted with pUC18 or pUC19 DNA at room temperature in air and low light for all reactions. The concentration of complex used and conditions of the experiment are given in the figure legends. A buffer solution (50 mM phosphate and 10 mM NaCl, pH 7.2) was used to bring the total volume to 40 μL. As a rule, buffer was added first, then the reagents and RPC, and finally the plasmid DNA. Reactions were quenched by placing the samples in an ice bath (dry ice and acetone). Plasmid reaction products were analyzed by addition of 10 μL of 6x loading buffer (30% glycerol in water with 0.1% w/v bromophenol blue) to the sample, vortexing, and loading 10 μL per well. The 1% agarose gels, containing ethidium bromide, were run in TAE buffer (40 mM tris-acetate, 1 mM EDTA, pH 8) at 5 V/cm (60 V) for 2 h and imaged using a Bio Rad Gel Doc™ XR+. Experiments in which scavengers, SOD, catalase, or other modifiers were used, the concentration is noted in the figure caption.

2.2.3 DNA Scission products assay

Reactions were conducted under the following conditions, (45.5 mL) 700 μM ctDNA, (4.1 mL) 58.3 μM (**4**$^{4+}$), (19.9 mL) 5.8 mM GSH, (30.5 mL) 50 mM phosphate, 10 mM NaCl Buffer at pH 7.4. Samples were digested at room

temperature in air overnight, then heated at 90 °C for 1 h in a GC oven. The reaction was quenched with ice bath (dry ice and acetone), extracted with 20 mL dichloromethane (DCM) 3x, dried with $MgSO_4$ and concentrated. Samples were resuspended in pure MeCN for HPLC analysis. The mobile phase of for HPLC was 0.1 TFA/MeCN 90/10, flow rate: 0.1 mL/min , injection vol: 10 μL, stationary phase: Zorbax Eclipse XDB-C18 4.6x150 column. The same method was conducted for $\mathbf{3}^{2+}$.

2.2.4 Cultured Cells, Materials and Methods

All solvents were reagent and cell culture grade. All reagents and work environments were maintained sterile. H358, HOP-62 and HCC2998 cells were purchased from The National Cancer Institute (NCI) at Frederick Central Repository. Hs766T cells were purchased from American Type Culture Collection (ATCC). RPMI-1640 and DMEM medium, penicillin/streptomycin, fetal bovine serum (FBS), 100X BME vitamin solution, bovine serum albumin (BSA), para-formaldehyde, methanol, sodium azide, dimethyl sulfoxide (DMSO), 0.04% trypan blue and 3-(4,5-dimethylthiazol-2-yl)-2,5-diphenyltetrazolium bromide (MTT) were purchased from Sigma Aldrich. Phosphate buffered saline 10X was purchase from Biorad. The DNA double strand break (DSB) γH2AX monoclonal antibody was purchased from EMD Millipore and Goat anti-mouse IgG (H+L) secondary antibody Alexa Fluor488 and Pro-gold anti-fade mounting agent were purchased from Invitrogen.

2.2.5 Cell Culturing and Experimentation

Cell incubation was maintained by a Thermofisher HeriCell CO_2 Incubator. Hypoxic incubation was maintained by a New Brunswick Galaxy 14s Dual Channel CO_2/N_2 incubator. Confocal microscopy was performed using a Zeiss Axio-Plane 540 with mercury lamp and argon laser. Absorbance readings were obtained using a BMG Labtech FLUOstar Omega plate reader.

2.2.5.1 Cell Culture

H358, HOP-62 and HCC-2998 cells were grown in RPMI-1640 medium supplemented with 10% FBS, 2 mM L-Glutamine, 1 mM sodium pyruvate, 1.1% penicillin/streptomycin and 1X BME vitamin complex solution. Hs766T cells were grown in DMEM medium supplemented with 10% FBS, 2 mM L-Glutamine, 1 mM sodium pyruvate, 1.1% penicillin/streptomycin and 1X BME vitamin complex solution. Cells were grown and passaged in T-25 and T-75 Corning culture flasks at 37 ^{o}C under 5% CO_2 and humidified atmosphere. Cells grown in hypoxic induced stress environments were grown and passaged in T-25 and T-75 Corning culture flasks at 37 ^{o}C under 5% CO_2 , 1.1% O_2 and humidified atmosphere.

2.2.5.2 Hypoxic and Normoxic Cell Viability

Cytotoxic effects of complexes $\mathbf{3}^{2+}$ and $\mathbf{4}^{4+}$ were tested on cell growth populations of H358, HCC-2998, HOP-62 and Hs766T. Normoxic [O_2] levels were adjusted to 18% in atmosphere and hypoxic [O_2] levels were adjusted to

1.1% in atmosphere in two separate incubation environments, the latter using a New Brunswick Galaxy 14s Dual Channel CO_2/N_2 incubator. Under aerobic conditions, cells were passaged and seeded onto 96 well plates. Plates were then placed in either a normoxic or hypoxic incubator and left to grow for 24 h. At this time, cells were inoculated with complexes $\mathbf{3}^{2+}$ and $\mathbf{4}^{4+}$ at titrating doses and placed back in their respective incubators for 72 h, after which the plates were removed and immediately assayed with MTT (5 mg/mL) for 3.5 h. Plates were read at 570 nm for absorbance of formazan production in the supernatant.

2.2.5.3 Measurement of intracellular ROS

The generation of ROS in H358 cells was measured using a ROS sensitive fluorescent probe, 2,7-dichlorodihydrofluorescein diacetate (DCFH-DA). DCFH-DA can be oxidized to 2′,7′-dichlorofluorescein (DCF) by ROS and exhibits green fluorescence intensity.[102] H358 cells were seeded on 25x25 mm microscope cover glass slips in BD Falon 60 x 60 mm tissue culture dishes for 72 h. Untreated cells were maintained as the negative controls whereas 10, 20 and 30% H_2O_2 solution in PBS was administered to cells for 15 minutes as positive controls.[75] H358 cells were also dosed with IC_{50} values of various complex as follows: $\mathbf{4}^{4+}$ (15 µM), $\mathbf{3}^{3+}$ (13 µM) and $\mathbf{2}^{2+}$ (1.7 µM) for 3 time periods of 2, 8, and 22 h. The cells were passaged and washed 3X in ice cold PBS then suspended in 10 mM DCFH-DA in PBS and incubated in the dark for 30 min. The levels of intracellular ROS were examined by confocal microscopy using long pass light

filters and a 1.3 airy unit pinhole at 488/529 nm with a Zeiss axio-plane inverted fluorescence microscope.

2.2.5.4 ATM Pathway Response Assay

H358 cells were seeded on 25x25 mm microscope cover glass slips in BD Falon 60 x 60 mm tissue culture dishes for 72 h. Cells were then treated with: etoposide (6 μM), $\mathbf{3}^{2+}$ (13 μM) and $\mathbf{4}^{4+}$ (15 μM) at their respective IC_{50}'s for 2, 8, and 22 h. The cover slips were removed and washed 3X in ice-cold phosphate-buffered saline (PBS) to remove residual drug. Cells were fixed with 4% para-Formaldehyde solution, permeabilized with 0.25% Triton and blocked with 3% BSA, anti-phospho ATM (phospho s1981) (1:1000) in 3% BSA/1% sodium azide was administered for 1.5 h in the dark at room temperature. Cells were then washed 3X in ice-cold PBS and Goat anti-rabbit IgG (H+L) secondary antibody Alexa Fluor488 (1:2000) in 3% BSA/1% sodium azide was administered for 3 h in the dark at room temperature. Cells were then treated with propidium iodide (5 mg/mL) for 5 min. After washing 3X with ice-cold PBS, the cells were fixed on microscope slide with Pro-Gold antifade reagent. Confocal microscopy was performed using long pass light filters and a 1.3 airy unit pinhole at 488/514 nm. 60x oil immersion objectives were used and digital camera images (DCIM) were captured using ZEN software.

2.2.5.5 γH2AX Double Strand Break Assay.

H358 cells were seeded on 25x25 mm microscope cover glass slips in BD Falon 60x60 mm tissue culture dishes for 72 h. Cells were then treated with complexes: etoposide, **3**$^{2+}$ and **4**$^{4+}$ at their respective IC_{50}'s for 2, 8, and 22 h. The cover slips was removed and washed 3X in ice-cold phosphate-buffered saline (PBS) to remove residual drug. Cells were fixed with 4% para-Formaldehyde solution, permeabilized with 0.25% Triton and blocked with 3% BSA, anti-phospho-histone (Ser139) γH2AX (1:1000) in 3% BSA/1% sodium azide was administered for 1 h in the dark at room temperature. Cells were then washed 3X in ice-cold PBS and Goat anti-mouse IgG (H+L) secondary antibody Alexa Fluor488 (1:2000) in 3% BSA/1% sodium azide was administered for 2 h in the dark at room temperature. Cells again were washed 3X in ice-cold PBS and then fixed on microscope slide with Pro-Gold antifade reagent. Confocal microscopy was performed using long pass light filters and a 1.3 airy unit pinhole at 488/519 nm. 60x oil immersion objectives were used and digital camera images (DCIM) were captured using ZEN software. Cell sorting and foci count were analyzed with Image J software for an average of 25 cells per image count.

2.3 RESULTS

2.3.1 DNA-Binding and Cleavage Activity

RPCs $\mathbf{1}^{2+}$ and $\mathbf{2}^{2+}$ bind predominantly via electrostatics with a binding constant on the order of 10^3 M^{-1}, the remainder $\mathbf{3}^{2+}$- $\mathbf{8}^{4+}$, with large planar aromatic units:

dppz (dipyrido[3,2-a:2',3'-c] phenazine), tpphz (tetrapyrido[3,2-a:2'3'-c:3'',2''-h:2''',3'''-j] phenazine), tatpp (9,11,20,22 -tetraazatetrapyrido[3,2-a: 2',3'-c: 3",2" -1: 2"',3"'-n] -pentacene), tatpq (9,11,20,22 -tetraazatetrapyrido[3,2-a: 2',3'-c: 3",2" -1: 2"',3"'-n] -pentacene-10,21-quinone, bind more tightly due to intercalation and exhibit binding constants in the range of 10^5 to 10^8 M^{-1}.[103,104]

RPC binding to DNA does not generally equate with RPCs causing damage. In the absence of deliberate irradiation to access the excited state chemistry of these complexes, the vast majority do not cause any DNA damage after binding. In Figure 2, we assay the DNA cleaving activity of RPCs $\mathbf{1}^{2+}$, $\mathbf{4}^{4+}$, $\mathbf{5}^{4+}$, $\mathbf{6}^{2+}$, and $\mathbf{8}^{4+}$ using a plasmid cleavage assay under physiologically relevant conditions (50 mM phosphate, 10 mM NaCl, 5.8 mM GSH, pH 7.2, aerobic). In this experiment, we monitored the conversion of supercoiled plasmid DNA (Form I) to nicked, open circular (Form II) and double-strand cleaved linear (Form III) DNA by agarose gel electrophoresis. As seen in Figure 2, we contrast the cleavage activity of the tatpp complex $\mathbf{4}^{4+}$ and the tatpq complex $\mathbf{5}^{4+}$, with a number of structurally related RPCs. RPC $\mathbf{3}^{2+}$ also cleaves DNA under these conditions.[12] Control experiments lacking GSH showed no cleavage activity by any complex. The presence of circular over linear DNA indicates SSBs are

prevalent. Hydrolytic cleavage of the DNA was ruled out by treating samples of RPC/GSH cleaved DNA with the T4 ligase repair enzyme to see if the cleavage was reversible the presumption being that hydrolytic cleavage is reversible whereas DNA damaged by oxidation is not easily religated. The cleavage induced by RPC $\mathbf{3}^{2+}$, $\mathbf{4}^{4+}$, or $\mathbf{5}^{4+}$/GSH combinations was not reversible (see SI, Figure S1 and S2), supporting oxidative DNA damage.

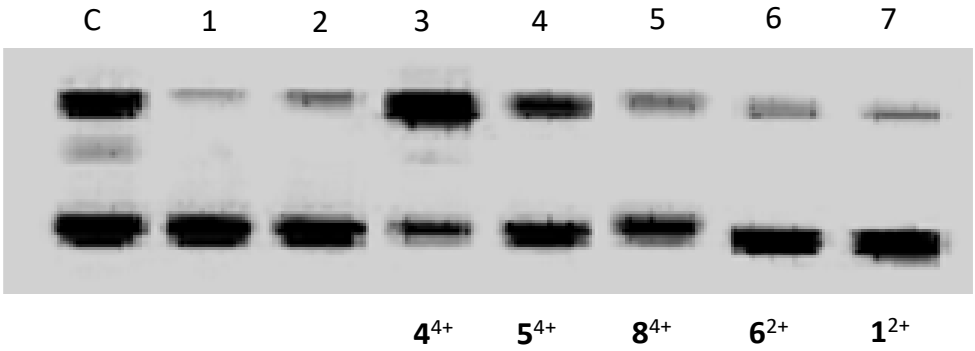

Figure 2 Agarose gel showing DNA cleavage products of pUC19 after treatment with RPCs 1–8 in the presence of GSH under aerobic conditions. Lane C, control showing open circular (Form II, top), linear (Form III, middle) and supercoiled (Form I, bottom) plasmid DNA. Lane 1, supercoiled plasmid DNA (144 μM DNA-bp) after 2 h incubation. Lane 2, supercoiled DNA (144 μM DNA-bp) with 120 μM GSH present after 2 h incubation. Lanes 3–7 supercoiled DNA (144 μM DNA-bp) with 12 μM RPC indicated and 120 μM GSH after 2 h incubation.

Activation by reduction is a common mechanism by which transition metal complexes activate O_2 to form ROS, but the redox processes typical for RPCs are generally not accessible by common cellular reductants or oxidants. For

virtually all RPCs, the first oxidative process is the $Ru^{2+/3+}$ couple which occurs at about 1.5 V vs NHE and is far too positive to be accessed in water or more pointedly in vivo (via non-photochemical pathways).[105] Reductions in RPCs are generally associated with ligand couples, such as the $[Ru^{II}(phen)_3]^{2+}/[Ru^{II}(phen)_2(phen^{\cdot-})]^{+}$ couple in which the electron is localized in one of the low-lying acceptor orbitals on the polypyridyl ligands, usually the LUMO. The potentials for these 'ligand-based' redox couples can vary dramatically with ligand structure. Figure 3 (bottom) shows a line graph of the observed first reduction potential for $\mathbf{1}^{2+}$ – $\mathbf{8}^{4+}$ as obtained in acetonitrile (see Table S1 in the supporting information). From this data, we observe that the phen and bpy ligands in RPCs $\mathbf{1}^{2+}$ and $\mathbf{2}^{2+}$ are the hardest to reduce at -1.1 V, followed by the dppz and tpphz ligands in $\mathbf{6}^{2+}$, $\mathbf{7}^{2+}$, and $\mathbf{8}^{4+}$ in the -0.76 to -0.5 V potential range, and finally the tatpp and tatpq ligands in $\mathbf{3}^{2+}$**,** $\mathbf{4}^{4+}$ and $\mathbf{5}^{4+}$ in the respective -0.1 to 0.05 V range (all potential are quoted vs NHE). It is clear that the RPC's with DNA cleavage activity, which are indicated by the circles filled with black dots (Figure 3, bottom), possess the most positive reduction potentials (>-0.2V vs NHE). With a reduction potential of -0.24 V (vs NHE, pH 7) for the glutathione disulfide/glutathione couple,[106] GSH can only reduce $\mathbf{3}^{2+}$, $\mathbf{4}^{4+}$ and $\mathbf{5}^{4+}$ of all the RPCs examined ($\mathbf{1}^{2+}$ – $\mathbf{8}^{4+}$) and it is no coincidence that these are the only RPCs observed to cleave DNA.

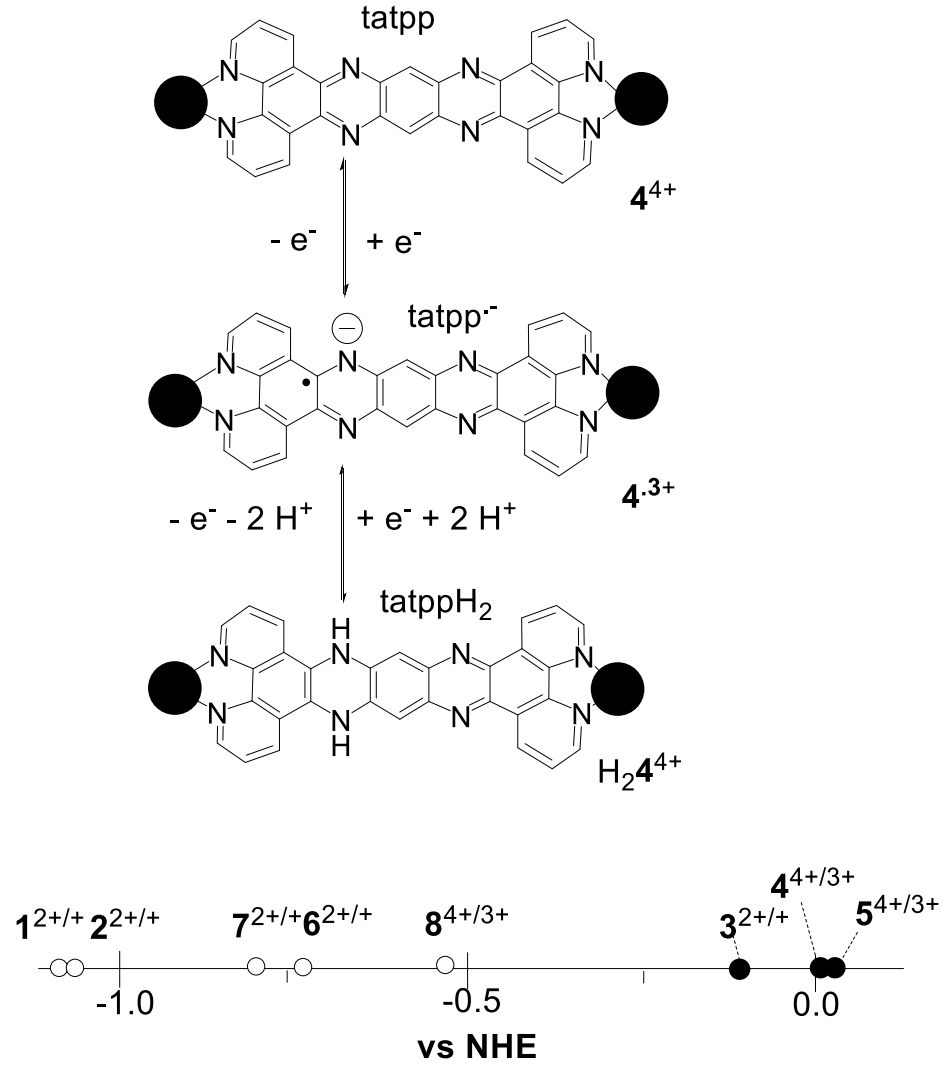

Figure 3 Top: Relevant redox isomers of $\mathbf{4}^{4+}$ in aqueous solution (pH 7.2). Black ball represents the $[Ru(phen)_2\}^{2+}$ fragment. Equivalent redox isomers exist for $\mathbf{3}^{2+}$ with respect to the tatpp ligand. Bottom: Plot of the first reduction potential for the RPCs $\mathbf{1}^{2+}$–$\mathbf{8}^{4+}$ in MeCN solvent. Open circles indicate complexes that are inactive for DNA cleavage and partially filled circles indicate complexes which cleave DNA in the presence of GSH.

Cleavage by O_2 activation could then be explained by GSH reduction of the RPC to a ligand radical species, shown for $\mathbf{4}^{4+}$ in reaction 1, which then reacts with O_2 to form superoxide, as shown in reaction 2. As $\mathbf{4}^{4+}$ is regenerated in reaction 2, it could then redox-cycle much like the related quinone-based anticancer drugs doxorubicin and daunorubicin to generate more ROS.[107-109] Superoxide is not potent enough to directly attack DNA but can form more potent ROS including H_2O_2 and hydroxyl radical through subsequent reductions. The involvement of hydroxyl radical in DNA cleavage was assessed by adding a number of

$$\mathbf{4}^{4+} + \tfrac{1}{2}\,\mathrm{GSH} \rightarrow \mathbf{4}^{\cdot 3+} + \tfrac{1}{2}\,\mathrm{GSSH} \qquad (1)$$

$$\mathbf{4}^{\cdot 3+} + O_2 \rightarrow O_2^{\cdot -} + \mathbf{4}^{4+} \qquad (2)$$

$OH^{\cdot}$ scavengers all of which attenuate the cleavage activity. Specifically, addition of sodium benzoate, sodium formate, mannitol, ethanol, or DMSO were all observed to inhibit the cleavage activity in a dose dependent manner for both $\mathbf{3}^{2+}$ and $\mathbf{4}^{4+}$ (see Supporting Information, Figures S3-7).[110,111] The gels (see SI Figures 3-7) were scanned by densitometry and the data reporting the relative amount of Form II nicked DNA are tabulated in Table 1. In addition to the observation of nicked DNA in agarose gels, large scale DNA cleavage reactions were extracted with dichloromethane and the characteristic small molecule by-products of deoxyribose degradation, 5-MF and furfural, could be identified by HPLC analyses (see SI Figure S11).[112,113] 5-MF and furfural are characteristic neutral byproducts of hydrogen atom abstraction from the C1 and C5

deoxyribose positions, respectively. Their presence indicates non-specific H atom abstraction and is supporting of hydroxyl radical as the active agent.

Table 1. Effect of cleavage activity with and without inhibitors at varying concentrations in the cleavage activity of $\mathbf{4}^{4+}$ and $\mathbf{3}^{2+}$ with GSH and plasmid DNA under aerobic conditions after 24 h incubation.

Inhibitor		% Form II cleavage from $\mathbf{4}^{4+}$ digestion	% Form II cleavage from $\mathbf{3}^{2+}$ digestion
Benzoate (mM)	0	74	74
	2	44	53
	4	33	40
	6	30	36
Formate (mM)	0	62	75
	2	44	57
	4	30	43
	6	27	39
Mannitol (mM)	0	67	71
	2	55	53
	4	39	49
	6	39	36
EtOH (mM)	0	71	79
	2	54	55
	4	39	46
	6	39	45
Pyruvate (mM)	0	74	78
	2	30	34
	4	31	28
	6	28	23
DMSO (mM)	0	64	74
	2	43	50
	4	34	37

DEF (mM)	6	31	31
	0	65	50
	2	26	19
	4	22	17
	6	22	17
SOD (μg/mL)	0	64	77
	15	39	50
Catalase (μg/mL)	0	67	75
	15	19	18
SOD and Catalase (μg/mL)	0	67	75
	15	20	20

Cleavage reactions in the presence of SOD and /or catalase revealed a central role for H_2O_2 over superoxide. As shown in Figure 5, addition of SOD attenuates but does not completely stop the cleavage activity of **4**$^{4+}$/GSH or **3**$^{2+}$/GSH aerobic mixtures whereas catalase does. The cleavage was also strongly attenuated upon addition of sodium pyruvate (see SI Figure S9), which is a selective scavenger for H_2O_2, further revealing H_2O_2 as an integral intermediate in the cleavage mechanism.[114,115] As SOD scrubs out superoxide and produces O_2 and H_2O_2, a basal level of cleavage activity would be expected if H_2O_2 were generated via this pathway and if H_2O_2 is the primary precursor to hydroxy radical. Catalase, which decomposes H_2O_2 to water and O_2, would completely arrest cleavage if H_2O_2 were the necessary precursor to hydroxy radical, as is observed.

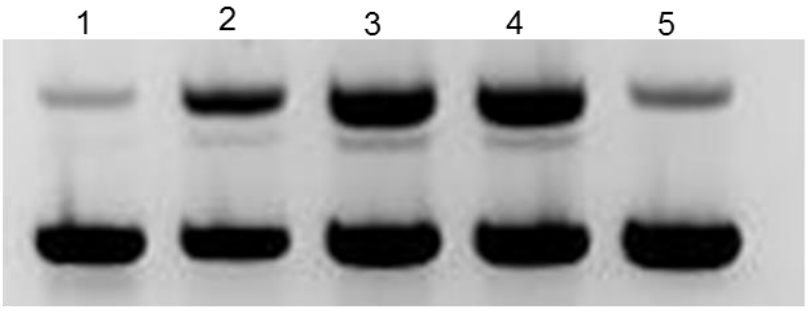

Figure 4 In vitro DNA plasmid cleavage assay in which pUC19 DNA (154 μM DNA-bp) was incubated with 4^{4+} (31 μM) in PBS buffer (pH 7.2) and 1.0 mM GSH at varying [O_2]. Lane 1: control, no **4**$^{4+}$, 220 mM O_2. Lane 2–5: DNA, **4**$^{4+}$, and varying amounts of O_2. Lane 4 also contains 30 μM 3,4-dihydroxybenzoate to show that this does not interfere with the assay lane 5 contains 30 μM 3,4-dihydroxybenzoate and 5 units of protocatechuate dioxygenase.

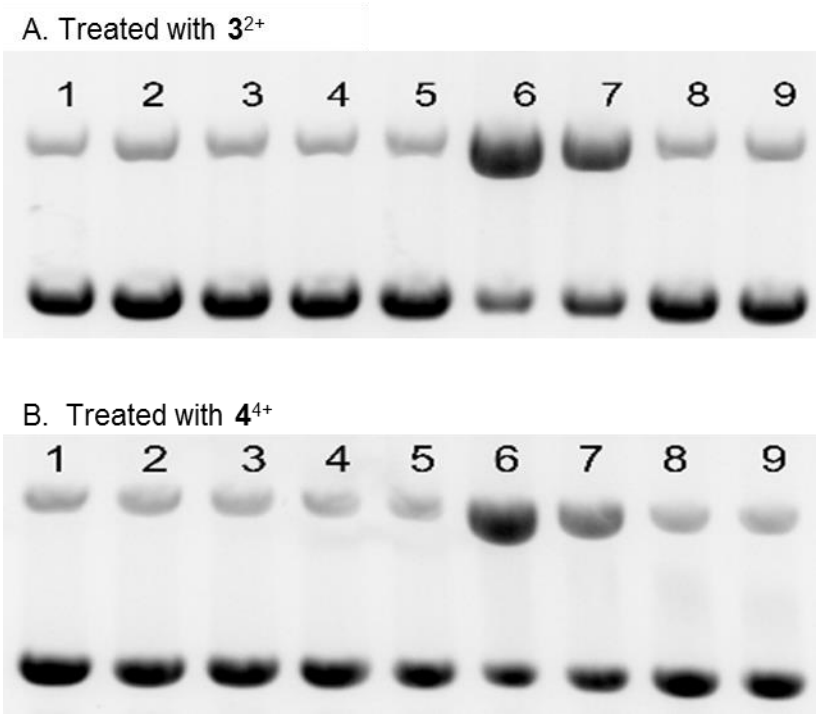

Figure 5 Effect of varying concentrations of SOD and catalase on the DNA cleavage activity of $\mathbf{3}^{2+}$ ((A) top gel) and $\mathbf{4}^{4+}$ ((B) bottom gel). Agarose gel (1%) stained with ethidium bromide of supercoiled pUC18 DNA (154 μM) cleavage products after incubation at 25 °C for 48 h with RPC (12.8 μM), GSH (256 μM) in 50 mM Na_3PO_4/10 mM buffer (pH 7.2). Lane 1: DNA control lane 2: GSH and DNA lane 3: DNA and RPC lane 4: SOD (15 μg mL−1) DNA lane 5: catalase (15 μg mL−1) and DNA lane 6: RPC, GSH and DNA lane 7: RPC, GSH, SOD (15 μg mL−1) and DNA lane 8: RPC, GSH, catalase (15 μg mL−1) and DNA lane 9: RPC, GSH, SOD (15 μg mL−1), catalase (15 μg mL−1) and DNA. All reactions were carried out under aerobic conditions.

Given the requirement for H_2O_2, reactions 1 and 2 do not explain the observed catalase inhibition, as reaction 2 only yields H_2O_2 indirectly, by either disproportionation, reaction 3, or by superoxide reduction by some other substrate. This latter reaction is limited, however, by the modest reduction potential of superoxide (+0.36 V at pH 7 and 25 C).[116] Disproportionation (rxn 2) should become slow at low $[O_2]$ as this would lead to low $[O_2^{\cdot-}]$, but as reported previously, DNA cleavage by $\mathbf{4}^{4+}$ was enhanced as the $[O_2]$ was lowered.[90] Oxygen concentrations were not quantitated in this previous study, so we examined the DNA cleavage activity of $\mathbf{4}^{4+}$/GSH

$$O_2^{\cdot-} + H_2O_2 \rightarrow HO^{\cdot} + HO^{-} + O_2 \qquad (3)$$

mixtures at three $[O_2]$. Aerobic solutions had a measured $[O_2]$ of 220 μM, as determined by an O_2 sensitive electrode. Solutions prepared in a nitrogen-filled glove box measured 4.0 μM $[O_2]$ and solutions in the nitrogen glove box and which were internally scrubbed by addition of protocatechuate 3,4-dioxygenase, and its substrate, 3,4-dihydroxybenzoate[117] showed no measureable $[O_2]$ by the O_2 sensitive electrode. As shown in Figure 4, considerably greater cleavage is observed for samples with 4.0 μM O_2 (lanes 3 and 4), compared to that under normoxic conditions (220 μM O_2, lane 2). However, no cleavage is seen in the absence of O_2 (lane 5). Lane 4 is a control in which 3,4-dihydroxybenzoate is present, and reveals this additive does not affect the DNA cleavage, nor does the protocatechuate 3,4-dioxygenase protein (data not shown).

With these data the question becomes, how does low [O_2] paradoxically favor enhanced DNA cleavage by ROS and how is H_2O_2 produced? Both of these questions can be explained by consideration of the multiple accessible and reversible redox states present in RPCs $\mathbf{3}^{2+}$, $\mathbf{4}^{4+}$ and $\mathbf{5}^{4+}$. As shown in Figure 3 (top), $\mathbf{4}^{4+}$ can undergo a single reduction to form the radical complex $\mathbf{4}^{\cdot 3+}$, or two reductions, accompanied by protonation at pH 7.2, to yield the diamagnetic complex $H_2\mathbf{4}^{4+}$ (shown as the benzoid tautomer).[118] These three isomers are analogous to the quinone, semiquinone radical, and hydroquinone isomers seen in the anthracyclines above, but based on reversible imine/amine couples.

A mechanistic pathway consistent with these results is shown in Scheme 1, which details a multistep pathway by which O_2 is activated to form superoxide and hydrogen peroxide upon redox cycling by the RPC $\mathbf{4}^{4+}$ (or $\mathbf{3}^{2+}$). As indicated in the column on the left, RPC $\mathbf{4}^{4+}$ can bind to DNA and be interconverted between three redox states by reaction with GSH and O_2. The relative amount of a given redox isomer being dictated by the GSH/O_2 ratio under steady-state conditions. At low GSH/O_2, the steady-state concentrations are shifted to the more oxidized isomers whereas at low GSH/O_2 the opposite occurs. As $H_2\mathbf{4}^{4+}$ (or $H_2\mathbf{3}^{2+}$) can directly produce H_2O_2 in a single step via a 2-electron, 2-proton transfer to O_2 (reaction 4), circumstances which favor a greater steady state concentration of [$H_2\mathbf{4}^{4+}$] also favor H_2O_2

$$H_2\mathbf{4}^{4+} + O_2 \rightarrow H_2O_2 + \mathbf{4}^{4+} \qquad (4)$$

production. Now the enhanced DNA cleavage activity under low [O_2] can be rationalized in terms of the enhanced efficiency at producing H_2O_2 relative to superoxide under hypoxia-like conditions. The direct production of H_2O_2 from the oxidation of hydroquinones,[119,120] polyphenols,[121] dihydroflavins,[122,123] and even dihydropyrazines[124] is well established.

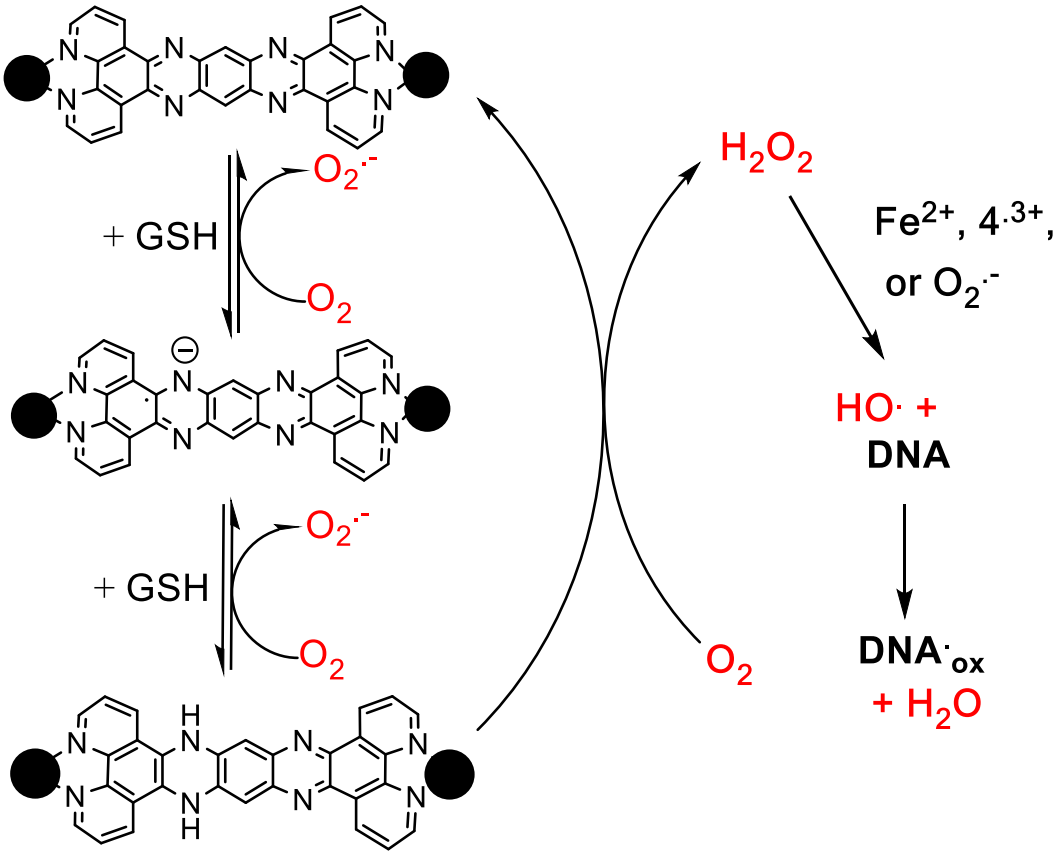

Scheme 1

Given the situation in which H_2O_2 production increases as the $[O_2]$ is lowered, enhanced DNA cleavage is explained by the H_2O_2 activation via Fenton chemistry (Reaction 5)[125] or reactions with other reductants, such as reactions 6 and 7, to yield the hydroxy radical. Adventitious Fe^{2+} is frequently observed to play a significant role in the activation of H_2O_2[125] and appears to play a role here. Addition of the iron chelator, deferoxamine,[126] to cleavage solutions of $\mathbf{4}^{4+}$ or $\mathbf{3}^{2+}$ and GSH and air mostly quenches the cleavage reaction (see SI Figure 10), suggests that trace Fe^{2+} is involved in the hydroxy radical production.

$$H_2O_2 + Fe^{2+} \rightarrow HO^{\cdot} + OH^- + Fe^{3+} \qquad (5)$$

$$O_2^{\cdot -} + H_2O_2 \rightarrow HO^{\cdot} + HO^- + O_2 \qquad (6)$$

$$\mathbf{4}^{\cdot 3+} + H_2O_2 \rightarrow \mathbf{4}^{4+} + HO^{\cdot} + HO^- + O_2 \qquad (7)$$

Reaction 7 shows that the radical $\mathbf{4}^{\cdot 3+}$ (or $\mathbf{3}^{\cdot 2+}$) can also activate H_2O_2 in a manner analogous to the semiquinone radical of anthracyclines.[111,127,128] Assuming these RPCs are DNA bound, this would generate the hydroxy radical in the immediate vicinity of the DNA, possibly increasing potency.

It is important to emphasize the difference in this redox activity with that of other known ruthenium-based drugs which are activated by reduction. A number of Ru(III) drugs, such as KP-1019 and NAMI-A, are bioreduced in situ to form the 'active' Ru(II) drug.[30,31] This reduction is irreversible and the resulting Ru(II) is thought to form adducts with many cellular structures, resulting in apoptosis, however even today the exact cellular targets and mechanism of

action are not fully understood.[29,129,130] In contrast, the ruthenium(II) center in RPC $\mathbf{3}^{2+}$ and $\mathbf{4}^{4+}$, are essentially inert throughout the process. Instead, the tatpp ligand is the redox-active unit which redox cycles with GSH and O_2 to catalytically generate ROS, which is conceptually related to the redox-cycling of Cu(II)phen and Fe-Bleomycin.[31,131-133] However, again an important distinction remains in that Cu(II)phen and Fe-Bleomycin show a directly proportional relationship between the observed DNA cleavage activity and the $[O_]$, whereas RPC $\mathbf{3}^{2+}$ and $\mathbf{4}^{4+}$ show an inverse proportionality. This is due to the presence of two ligand-based redox couples, the doubly-reduced form being increasingly accessed as the GSH/O_2 ratio climbs and which can then react with the remaining O_2 to directly produce H_2O_2 with better efficiency. This unusual $[O_2]$ dependence could have utility in enhancing the treatment in hypoxic regions of tumors.

As a point of clarification, we have previously reported that the doubly-reduced $[H_2\mathbf{4}]$ Cl_4 cleaved DNA in the absence of both GSH and O_2.[90] Moreover, added 2,2,6,6-tetramethyl-1-piperdinyloxy (TEMPO) attenuated this cleavage while added DMSO did not. TEMPO can quench carbon-based radical species[134,135] whereas DMSO is primarily a scavenger for ROS.[5,126,136] At that time, we were using a nitrogen glove box for ‘anaerobic‘ work for which we now know leads to solutions with measurable $[O_2]$. Once this was understood, we assumed that ROS were responsible for the observed cleavage, however, this is at odds with the cleavage activity observed in the presence of DMSO. Another possibility, that we still need to demonstrate, is oxidation of $H_2\mathbf{4}^{4+}$ by O_2 leads to some DNA-bound $\mathbf{4}^{\cdot 3+}$. This radical persists for long periods in intimate contact

with the DNA (and we know this radical is remarkably stable[137,138]) and possibly can directly abstract a H-atom from the deoxyribose unit. Such dual cleavage mechanisms (O_2 dependent and O_2 independent) are precedented in the related antibiotic anthraquinones, daunorubicin and doxorubicin,[108,139] and DNA cleaving-dihydropyrazines,[124,140-143] both which form DNA bound radical species that can either activate O_2 or directly attack the DNA.

2.3.2 ROS production and DNA cleavage activity in cultured human cancer cells

The inhibitory concentrations 50% (IC_{50}) for many of the RPCs in cultured human NSCLC H358 cells are reported in Table 2 and were determined using the MTT assay. In general, RPCs that are not redox-active and which do not induce DNA cleavage in cell-free assays, as described previously, are less cytotoxic. The clear exception being RPC $\mathbf{2}^{2+}$, which is the most potent of all those examined, with an IC_{50} of 1.7 μM. RPCs $\mathbf{3}^{2+}$ and $\mathbf{4}^{4+}$ were the next most potent at 13-15 μM. We have previously shown that H358 cells treated with $\mathbf{3}^{2+}$ or $\mathbf{4}^{4+}$ (5 μM) for as little as 1 hour have appreciable quantities of ruthenium in both the whole cell and nuclear fractions, as detected by graphite furnace atomic absorption spectroscopy, revealing facile transport into the cells and nucleus.[75] RPC $\mathbf{2}^{2+}$ is well-known for its cytotoxic properties and is found to localize in lysosomes and mitochondria.[24] It's cytotoxicity is largely been attributed to mitochondrial poisoning.[24]

Table 2. IC_{50} values for RPCs against H358 Cells (chloride salts)

Compound (RPC)	Abbr	H358 IC_{50} (μM)	Ref
$[Ru(phen)_3]^{2+}$	1^{2+}	86.7 ± 4.1	[97]
$[Ru(Ph_2phen)_3]^{2+}$	2^{2+}	1.7 ± 0.1	This work
$[(phen)_2Ru(tatpp)]^{2+}$	3^{2+}	13.2 ± 1.8	[97]
$[(phen)_2Ru(tatpp)Ru(phen)_2]^{4+}$	4^{4+}	15.2 ± 1.8	[97]
$[(phen)_2Ru(dppz)]^{2+}$	6^{2+}	35.1 ± 0.71	This work
$[(phen)_2Ru(tpphz)]^{2+}$	7^{2+}	44.0 ± 3.0	[97]
$[(phen)_2Ru(tpphz)Ru(phen)_2]^{4+}$	8^{4+}	41.8 ± 2.7	[97]

H358 cells treated with RPC $\mathbf{4}^{4+}$ (15 μM) and to a lesser extent, $\mathbf{3}^{2+}$, (13 μM) show significantly elevated ROS levels in within 2 hours of treatment as observed using a fluorescent ROS-sensitive dye, DCFH-DA,[144] and fluorescent microscopy. DCFH-DA is an oxidation sensitive dye that fluoresces brightly and is measured in the green when intracellular ROS is generating in a cell.[75,145,146] DCFH-DA was commonly and inaccurately thought to be a H_2O_2 specific marker but more recently shown to be a more general ROS detection dye, as it is also sensitive to superoxide ion.[145,147] As shown in Figure 6, the green fluorescence image tracks indicate ROS production within the H358 cells treated with H_2O_2, RPCs $\mathbf{3}^{2+}$, $\mathbf{4}^{4+}$ and $\mathbf{2}^{2+}$, or untreated cells. The negative control shows the basal levels of ROS whereas the positive control shows the dye activity in the presence

of H_2O_2, principally in the cytoplasm. Cells treated with RPC $\mathbf{2}^{2+}$ (1.7 μM) represent a negative control in that this RPC, while quite cytotoxic, does not redox-cycle nor generate ROS unless specifically irradiated with light,[40,47,148] which is avoided here. Comparisons of the columns in which RPCs $\mathbf{3}^{2+}$, $\mathbf{4}^{4+}$ and $\mathbf{2}^{2+}$ were used show that RPC $\mathbf{4}^{4+}$ clearly promotes significant ROS production in cells after only 2 h incubation, whereas RPC $\mathbf{3}^{2+}$ does elevate ROS production also, but less dramatically so. At longer incubation periods (22 h), both $\mathbf{3}^{2+}$ and $\mathbf{4}^{4+}$ generate substantial amounts of ROS intracellularly. RPC $\mathbf{2}^{2+}$ does not result ROS production over the basel level at 2 or 8 h. At 22 h, the increase can be largely attributed to indirect pathways to ROS production as the cytotoxic activity results in activation of apoptotic pathways. Most significantly, the ROS activity seen in the gel-shift assays for $\mathbf{3}^{2+}$ and $\mathbf{4}^{4+}$ and the lack of activity for $\mathbf{2}^{2+}$ are clearly mirrored here

.

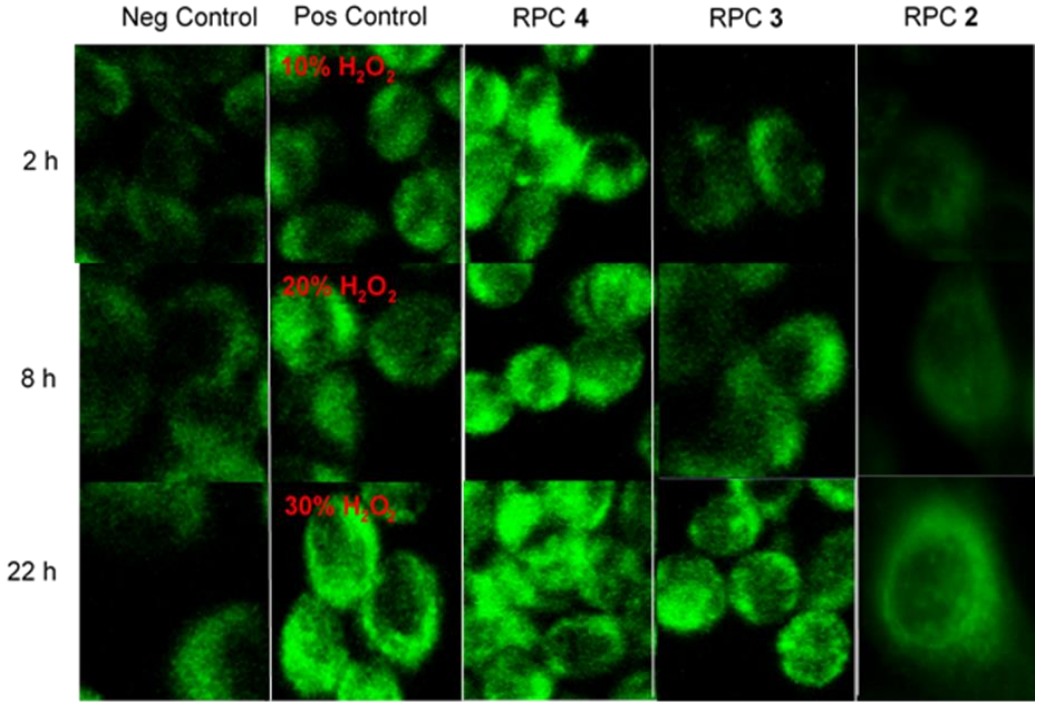

Figure 6 H358 cells stained with DCFH-DA to image ROS production. First column is untreated cells as a negative control. Second column is the positive control where cells were dosed with 10, 20, and 30% solutions of H_2O_2 for 15 min and imaged with DCFH-DA. Third, fourth, and fifth columns show H358 cells dosed with relative IC50 values of various complex as follows: $\mathbf{4}^{4+}$ (15 μM), $\mathbf{3}^{3+}$ (13 μM) and $\mathbf{2}^{2+}$ (1.7 μM) for the 3 time periods indicated. DCFH-DA was then administered for 30 min and imaged using confocal microscopy (488/519 nm).

2.3.3 DNA cleavage activity in cultured human cancer cells

The single strand DNA cleavage observed cell-free assays and the ROS activity seen in cells, is observed to lead to DSBs in H358 cells. Oxidative DNA damage in the form of DSBs could be detected by monitoring the appearance of the phosphorylated protein, ataxia-telangiectasia mutated (pATM) and its downstream effect, γH2AX, in the nuclei of treated cells using immunofluorescent (IF) stains.[149-151] DSBs induced by a number of causes including ionizing radiation and ROS are known to activate ATM.[152] As seen in Figure 7, nuclear DSBs show up as green foci upon fixing and staining cells with ATM primary antibody where the nucleus of each cell is stained with propidium iodide (PI). Each track in the series shows the merged signals of ATM and PI. Etoposide was used as a positive control, as it is known to stabilize transient covalent complexes between topo 2 and DNA, ultimately converting them to DSBs in the S-phase cell cycle.[153,154] As seen in Figure 7, cells treated with the IC_{50} dose of $\mathbf{4}^{4+}$ and etoposide (1 μM) show numerous foci representing DSBs recruiting ATM at 2 h which become ever more present at longer time periods, 8 and 22 h, respectively. Cells treated with the IC_{50} dose of $\mathbf{2}^{2+}$ and $\mathbf{3}^{2+}$ show no or little pATM foci at 2 h, respectively, and while foci become apparent for $\mathbf{3}^{2+}$ at 8 and 22 h, they are never observed for cells treated with $\mathbf{2}^{2+}$ (up to 22 h). Again we observe distinctly different outcome for redox-active versus redox-inactive RPCs, with a noticeable lag in the activity in $\mathbf{3}^{2+}$ compared to $\mathbf{4}^{4+}$.

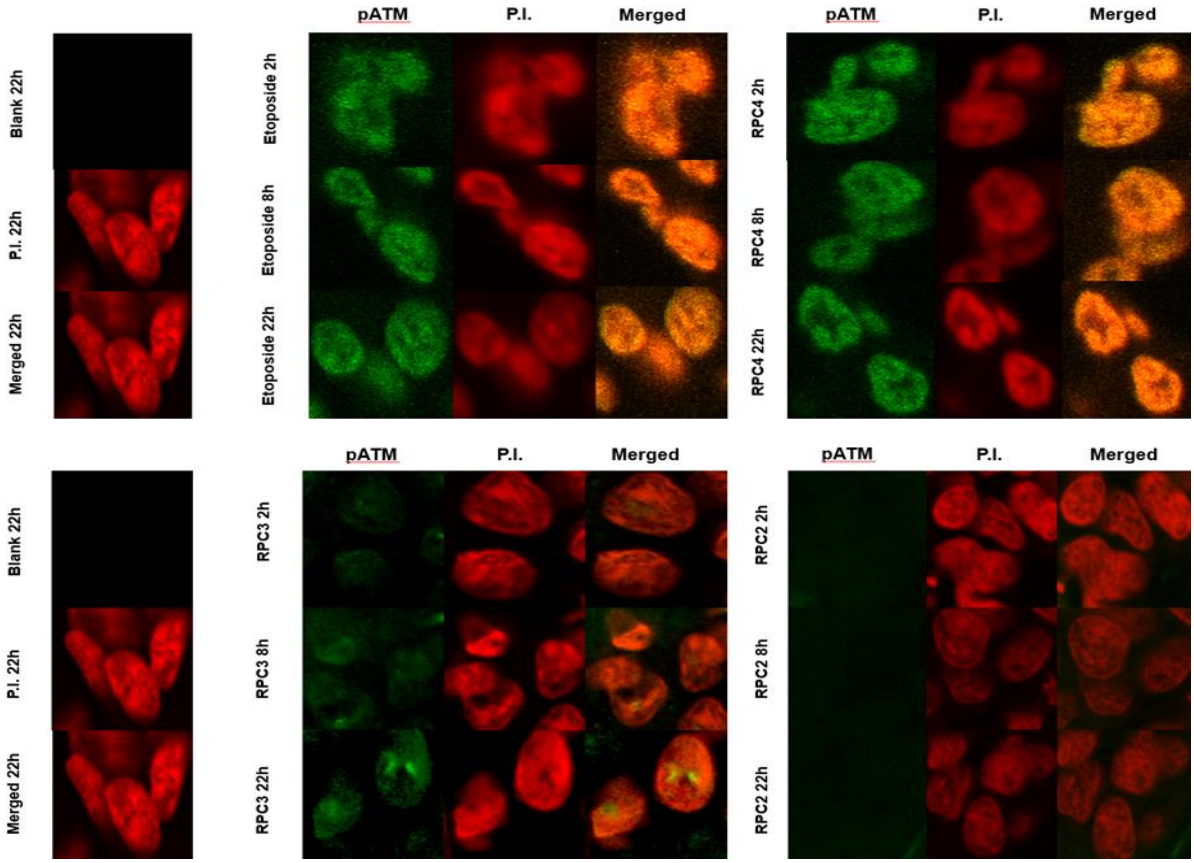

Figure 7 Immunofluorescence staining of pATM foci in H358 cell line. The cells were fixed stained and imaged at 2, 8, and 22 h post treatment with the IC50 values for $\mathbf{4}^{4+}$ and $\mathbf{3}^{2+}$.

DSBs also cause damage at associated loci on the histone cause the histone ser-139 residues in mammalian cells to be phosphorylated which can be directly detected using the γH2AX assay.[141] DSBs after activation of ATM recruits the downstream phosphorylation of γH2AX and show up as yellow-green foci

upon fixing and staining H358 cells with γH2AX primary antibody. For a positive control, H358 cells were irradiated (IR) with 1.8 Gy and show numerous DSB foci within 30 minutes[154,155 156-158] and is compared to the negative control of untreated H358 cells, which is dark (Figure 8, left). As in our ATM assay, etoposide was used again as a positive control for DSB formation and in Figure 8, cells treated with the IC_{50} dose (1.0 μM etoposide) show again numerous DSBs at 2 h which become substantial at longer time periods, 8 and 22 h, respectively.[153,154] The next two columns in Figure 8 show similar nuclear effects upon treating H358 cells with **4**$^{4+}$ (15 μM) and **3**$^{2+}$ (13 μM) at their IC_{50} dose. Cells treated with **4**$^{4+}$ mimicked etoposide with numerous DSBs evident after the 2 h time period and even greater increases seen in the foci count with increasing time. In tandem with the ATM assay, RPC **3**$^{2+}$ showed substantially fewer DSBs at the 2 and 8 h time points, than seen for etoposide or **4**$^{4+}$. At 22 h, the appearance of numerous DSBs could be attributed to an indirect mechanism and an apoptotic cascade, however it is notable that no DSBs are seen in the nuclei of cells treated with **2**$^{2+}$, even at 22 h. This data reveal very different mechanisms of action for **4**$^{4+}$ versus **2**$^{2+}$ and hint that the mechanism of action for **3**$^{2+}$ may deviate from **4**$^{4+}$. It is hard to attribute the strong 2 h DSB response seen in cells treated with **4**$^{4+}$ to anything other than a direct response, which is mirrored by other agents directly acting on the nuclear DNA (etoposide and radiation) and these DSBs represent the primary event responsible for apoptosis.[159,160]

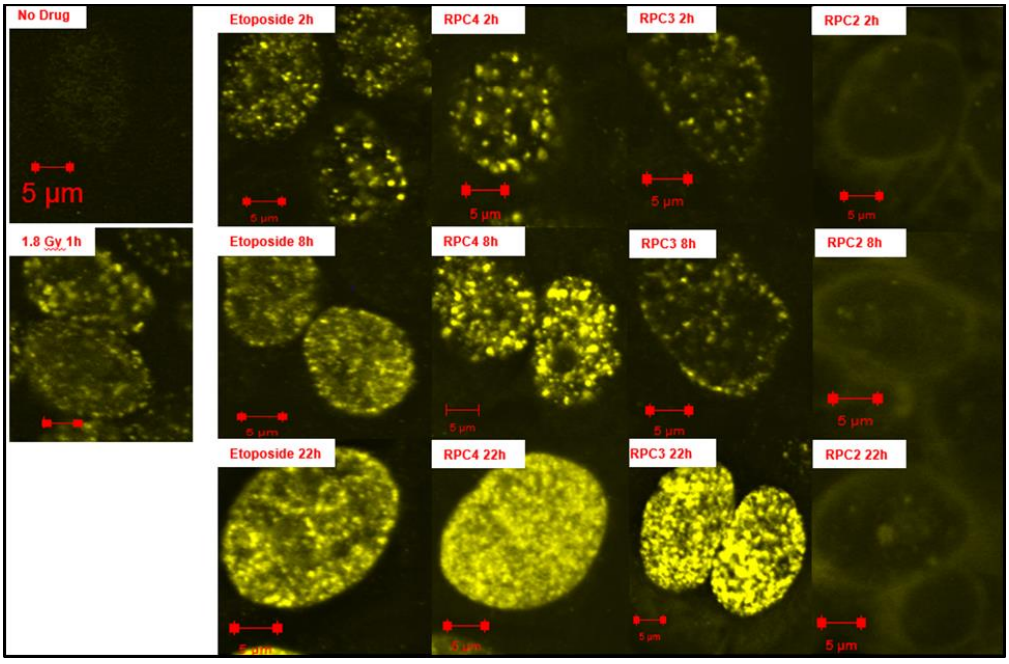

Figure 8 Immunofluorescence staining of γH2AX foci in H358 cell line. The cells were fixed stained and imaged at 2, 8, and 22 h post treatment with the IC50 values for $\mathbf{4}^{4+}$ and $\mathbf{3}^{2+}$.

As shown in Figure 9, quantitation of the γH2AX foci (using the Image J software package with gives a count of the foci per 25 cells[161]) reveals that etoposide and $\mathbf{4}^{4+}$ show an equal response after 2 h, whereas $\mathbf{3}^{2+}$ is only slightly above the negative control. At 8 h, $\mathbf{4}^{4+}$ shows more foci than etoposide and almost 5 fold more foci than cells treated with $\mathbf{3}^{2+}$. Only after 22 h, do the foci count become near equal and the extensive number of foci (over 250 each) indicative of apoptosis. RPC $\mathbf{4}^{4+}$ clearly shows mechanistic similarities with other DNA cleavage agents and is competitive with etoposide. The DSBs for $\mathbf{3}^{2+}$, on

the other hand, indicate a potential divergence in their mechanistic pathway in cells, despite near identical behavior cell-free studies. This last result is particularly intriguing as both **3**$^{2+}$ and **4**$^{4+}$ are essentially equitoxic as measured by IC_{50} values to H358 cells, and show similar tumor growth inhibition in mouse tumor models.[12] Additional studies must be performed with **3**$^{2+}$ and **4**$^{4+}$ to determine if these divergent results are due to different transport rates and pathways, cellular localization, or simply different pro-apoptotic cascade pathways.

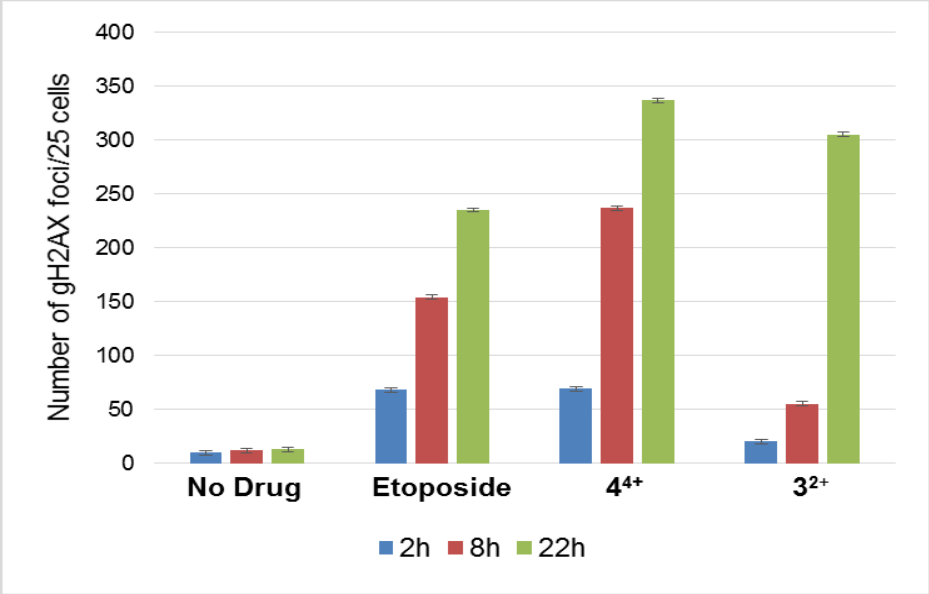

Figure 9. Quantitative analysis of γ-H2AX foci in H358 cell line for etoposide, **4**$^{4+}$, and **3**$^{2+}$ using image J software. An average of 25 cells per count were used in tandem with double phase light contrast particle count.

It is curious that SSBs are observed in cell-free assays, while DSBs are observed in cells. It is possible that the catalytic ROS activity of $\mathbf{3}^{2+}$ and $\mathbf{4}^{4+}$ leads to multiple SSBs resulting in DSBs, but it would be odd that this only occurs in cells. As these RPCs are known to intercalate, it could be that these RPCs induce other injuries to the cellular DNA, such as topoisomerase inhibition. In combination with the ROS generation, DSBs are effectively produced. The low cytotoxicity of other known metallointercalators with very similar structures, but lacking the redox cycling functionality (i.e., RPCs $\mathbf{6}^{2+}$, $\mathbf{7}^{2+,}$ and $\mathbf{8}^{4+}$ see Table 2) suggest that intercalation in the absence of ROS production is not sufficient for a substantial cytotoxic effect. Further supporting this, fluorescent imaging of MCF7 cells treated with RPC $\mathbf{8}^{4+}$ reveals this RPC does accumulate in the cell nuclei, yet it is relatively non-cytotoxic (MCF7 IC_{50} 138 μM).[42,43] We postulate that the combination of efficient ROS production in the immediate vicinity of the DNA and inhibition of normal nuclear DNA functions by intercalation result in DSBs in cells, whereas only SSBs are seen in cell-free assays where the family of DNA associated proteins are absent.

2.3.4 Effects of RPCs in Cancer Cells within a Hypoxic Environment

An examination of the cytotoxicity of $\mathbf{3}^{2+}$ and $\mathbf{4}^{4+}$ in H358, HCC2998, HOP-62, Hs766t was conducted under normoxia (18% O_2) and hypoxia (1.1 % O_2), to see if the O_2 sensitivity seen in vitro in observed in cells. The bar graphs in Figure 10 compare the IC_{50}, as measured by MTT assay, of $\mathbf{3}^{2+}$ and $\mathbf{4}^{4+}$ when the cells are incubated under normoxic conditions (blue) and hypoxic conditions

(red). A two-fold enhancement in cytotoxicity is seen for **3**$^{2+}$ in Hs766t and HOP-62 under hypoxia compared to normoxia, however, the remaining cell lines, H358 and HCC2998, showed little difference. Surprisingly, no difference was observed in the cytotoxicity of **4**$^{4+}$ in all four cell lines between normoxic and hypoxic conditions. Ultimately, it appears that even though DNA cleavage is enhanced in cell-free assays under hypoxic relative to normoxic conditions, the DNA damage done in cells under normoxic conditions is sufficient to trigger the same apoptotic response as seen under hypoxia. While this suggests the RPC **4**$^{4+}$ is not selective for hypoxic cell populations, the fact that the activity of **4**$^{4+}$ is not diminished under hypoxia is still quite attractive, as many anticancer drugs become less effective when cells are under hypoxic stress.[162,163]

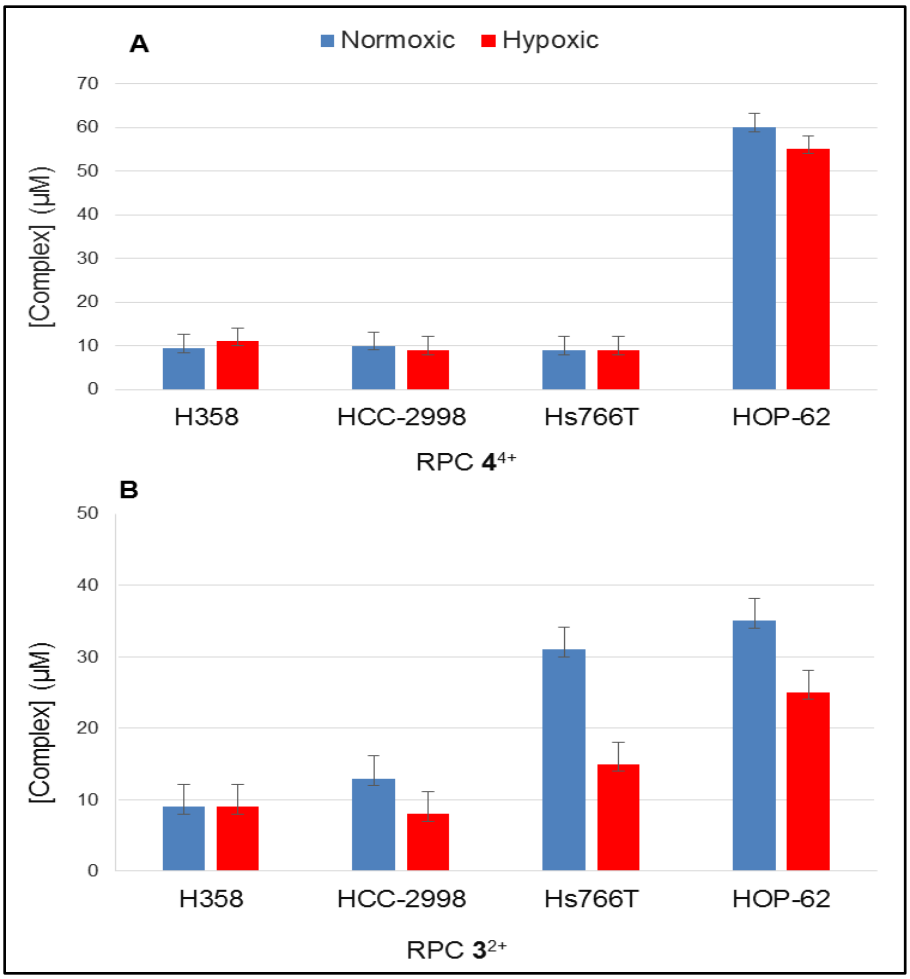

Figure 10. IC_{50} of human malignant cell lines treated with RPCs $\mathbf{3}^{2+}$ and $\mathbf{4}^{4+}$ under normoxia (18% O_2) and hypoxia (1.1 % O_2) represented by the blue and red bars respectively. In this case the enantiopure Δ-$\mathbf{3}^{2+}$ and $\Delta\Delta$-$\mathbf{4}^{4+}$ were used, which is why the IC_{50}'s reported under normoxia are lower. IC_{50}'s were determined using the MTT assay. Error bars indicate the standard deviation of IC_{50} as measured from three 96 well plates. Each plate contained six replicates at each concentration to determine the IC_{50}.

2.4 Conclusions

The cell-free data support a mechanistic model in which single-strand cleavage activity of DNA-bound $\mathbf{3}^{2+}$ and $\mathbf{4}^{4+}$ is observed due to redox-cycling mediated by the [GSH] and [O_2] . The [GSH]/[O_2] ratio dictates the steady state concentration of the three redox isomers of $\mathbf{3}^{2+}$ and $\mathbf{4}^{4+}$ in such a manner that at low [O_2] and high [GSH] , a pathway favorable to H_2O_2 production becomes increasingly favorable. The relative efficiency by which H_2O_2 can be activated to form hydroxy radicals over superoxide results in enhanced DNA cleavage under low O_2 conditions (assuming [GSH] is held relatively constant). This redox-cycling means that the RPCs are catalytic with respect to DNA cleavage. The tatpp ligand is key to this functionality and bears some resemblance to the intercalating anthraquinone anti-cancer drugs, which also show DNA damage via redox cycling. The metal fragments impart a similar DNA binding affinity to the RPCs as the anthraquinones and the tatpp ligand imparts the redox-cycling activity. It remains to be seen how these two classes of intercalators overlap in terms of specificity, toxicity, and spectrum of use and where they diverge.

The DNA cleavage activity of RPC $\mathbf{4}^{4+}$ and to a lesser extent $\mathbf{3}^{2+}$ is observed in the nuclei of H358 cells, however this time as DSBs. Within 2 h of treatment with an IC_{50} dose of $\mathbf{4}^{4+}$, H358 cells show elevated levels of ROS as detected by the fluorescent ROS-sensitive dye, DCFH-DA, marked phosphorylation of the ATM signaling protein in the nuclei indicating DNA damage in response to ROS, and direct observation of DSBs in the nuclei using the γH2AX assay. Cells treated with $\mathbf{3}^{2+}$ also show these responses, but with a 3 to 6

h temporal delay that could indicate an indirect cleavage mechanism and which could suggest divergent reaction mechanisms for $\mathbf{3}^{2+}$ and $\mathbf{4}^{4+}$ in live cells. Cells treated with the nonredox-active RPC $\mathbf{2}^{2+}$, which is even more cytotoxic towards H358, show none of these behaviors even after 22 h treatment, suggesting the redox cycling in $\mathbf{3}^{2+}$ and $\mathbf{4}^{4+}$ is integral towards thier function.

This correlation in activity between cell-free and cell studies is a first with ruthenium polypyridyl-based drugs, to our knowledge. It is interesting that the enhancement in cytotoxicity seen for RPC $\mathbf{3}^{2+}$ under hypoxia over normoxia is more pronounced than for $\mathbf{4}^{4+}$. While neither $\mathbf{3}^{2+}$ or $\mathbf{4}^{4+}$ is dramatically more cytotoxic under hypoxia if at all compared to normoxia, it is promising to note that they are not less effective under hypoxia, which is common to many O_2 activating drugs.

This work also demonstrates the importance of analyzing the temporal cellular effects of treating cells with RPCs. There are numerous reports explaining how RPCs, including RPC $\mathbf{2}^{2+}$, poison mitochondria or disrupt other cellular functions, however the conclusions are based on a single time point, meaning that the observed effect could be due to apoptotic cascades induced by the RPC at any number of locations.

2.5 ASSOCIATED CONTENT

2.5.1 Supporting Information Index

2.5.2 T4 Ligase Assay

Digested reactions with pUC19 DNA, GSH, **4**$^{4+}$ or **3**$^{2+}$ and phosphate buffer were treated with T4 ligase enzyme and buffer. All reactions had a total volume of 20 µL. To serve as a control pUC19 plasmid DNA was digested with EcoRI for two hours. The EcoRI mixture containing 5 µL water, 8 µL of RE 10X buffer, 0.8 µL acetylated BSA, 4 µL of pUC19 plasmid DNA and 2 µL of EcoRI was heat inactivated at 65 °C for ~20 minutes. Two reaction vials were made. Following heat inactivation 1.0 µL of T4 ligase 10X buffer and 0.5 µL of T4 DNA ligase was added to one of the two reaction vials to re-ligate the DNA for ~1 hour. Two reaction vials for both **3**$^{2+}$ and **4**$^{4+}$ were prepared as well. These reaction vials were prepared with samples prepped for the DNA agarose assay. However, to one of the vials containing **3**$^{2+}$ and one containing **4**$^{4+}$ was added 1.0 µL of T4 ligase 10X buffer and 0.5 µL of T4 DNA ligase. The reactions were digested for ~ 1 hour. All samples were then analyzed with DNA gel electrophoresis and 6X loading buffer.

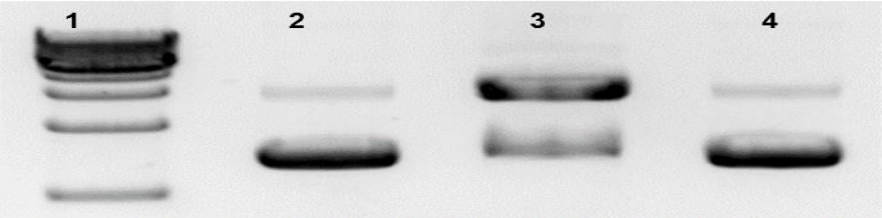

Figure S1. T4 ligase assay control.

Agarose gel (1%) stained with ethidium bromide of supercoiled pUC18 DNA (154 µM) cleavage products after incubation at 25 ^{o}C for 48 h with **4**$^{4+}$ (12.8 µM), GSH (256 µM) in 50 mM Na_3PO_4/10 mM buffer (pH 7.2). Where lane 1: is a 1kb DNA ladder lane 2: pUC19 DNA in buffer lane 3: pUC19 DNA treated with EcoRI, and lane 4: pUC19 treated with T4 ligase after EcoRI treatment.

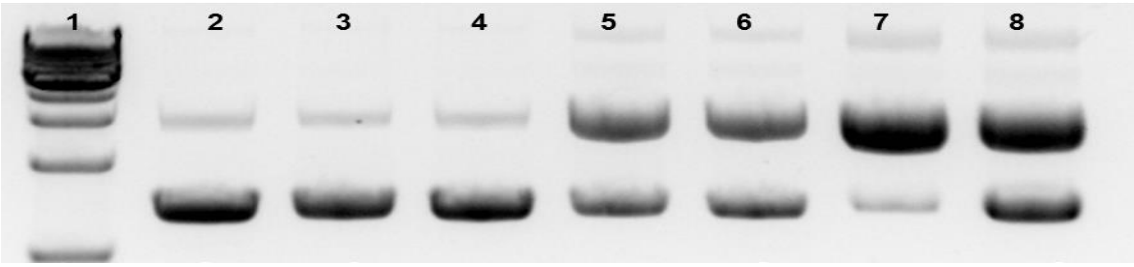

Figure S2.T4 ligase assay to show hydrolytic cleavage for **3**$^{2+}$ and **4**$^{4+}$

T4 ligase assay. Agarose gel (1%) stained with ethidium bromide of supercoiled pUC18 DNA (154 µM) cleavage products after incubation at 25 ^{o}C for 48 h with **4**$^{4+}$ (12.8 µM), GSH (256 µM) in 50 mM Na_3PO_4/10 mM buffer (pH 7.2). Where lane 1: is a 1 kb DNA ladder lane 2: pUC19 DNA in buffer lane 3: pUC19 DNA and **4**$^{4+}$with buffer lane 4: pUC19 DNA and **3**$^{2+}$ with buffer lane 5: **4**$^{4+}$, GSH and DNA Lane 6: **3**$^{2+}$, GSH and DNA Lane 7: same as lane 5 treated with T4 ligase lane 8: same as lane 6 treated with T4 ligase.

*2.5.3 Figures of DNA Cleavage Activity of **3**$^{2+}$ and **4**$^{4+}$ with Inhibitors*

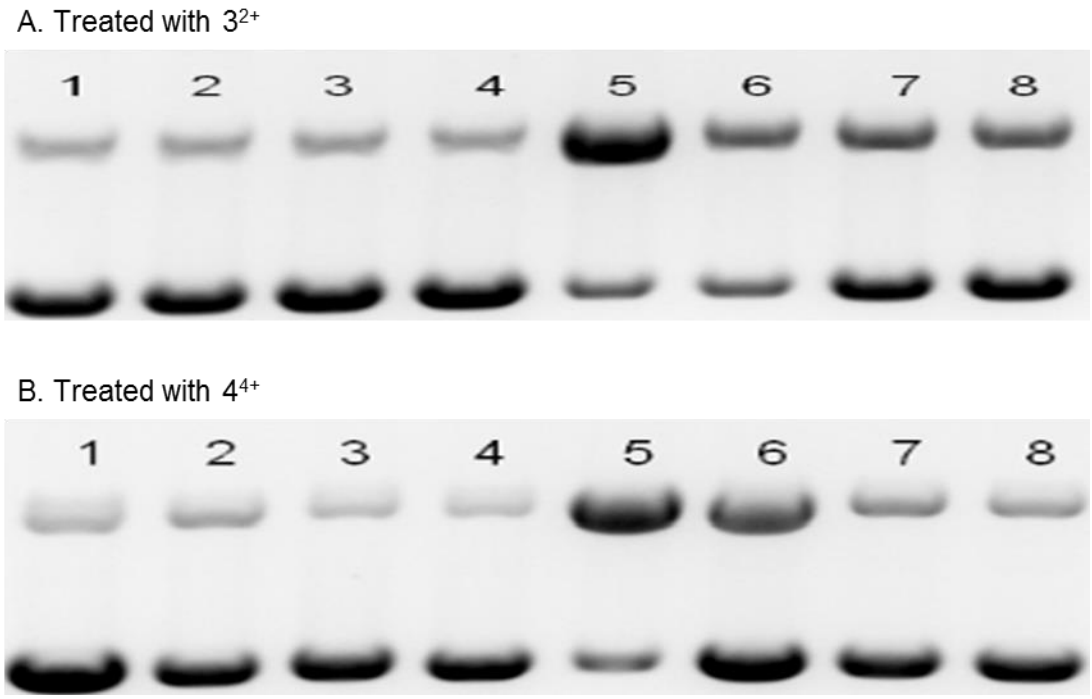

Figure S3. Effect of addition of varying concentrations of sodium benzoate to the DNA cleavage activity of **3**$^{2+}$ (A. top gel) and **4**$^{4+}$ (B. bottom gel). Agarose gel (1%) stained with ethidium bromide of supercoiled pUC18 DNA (154 µM) cleavage products after incubation at 25 ^{o}C for 48 h with RPC (12.8 µM), GSH (256 µM) in 50 mM Na_3PO_4/10 mM buffer (pH 7.2). Lane 1: DNA control Lane 2: GSH and DNA Lane 3: DNA and RPC Lane 4: sodium benzoate (6.4 mM) DNA Lane 5: RPC, DNA and GSH Lane 6: RPC, GSH, DNA and sodium benzoate (2.1 mM) Lane 7: RPC, GSH, DNA and sodium benzoate (4.2 mM) Lane 8: RPC, GSH, DNA and sodium benzoate (6.4 mM). All reactions were carried out under aerobic conditions.

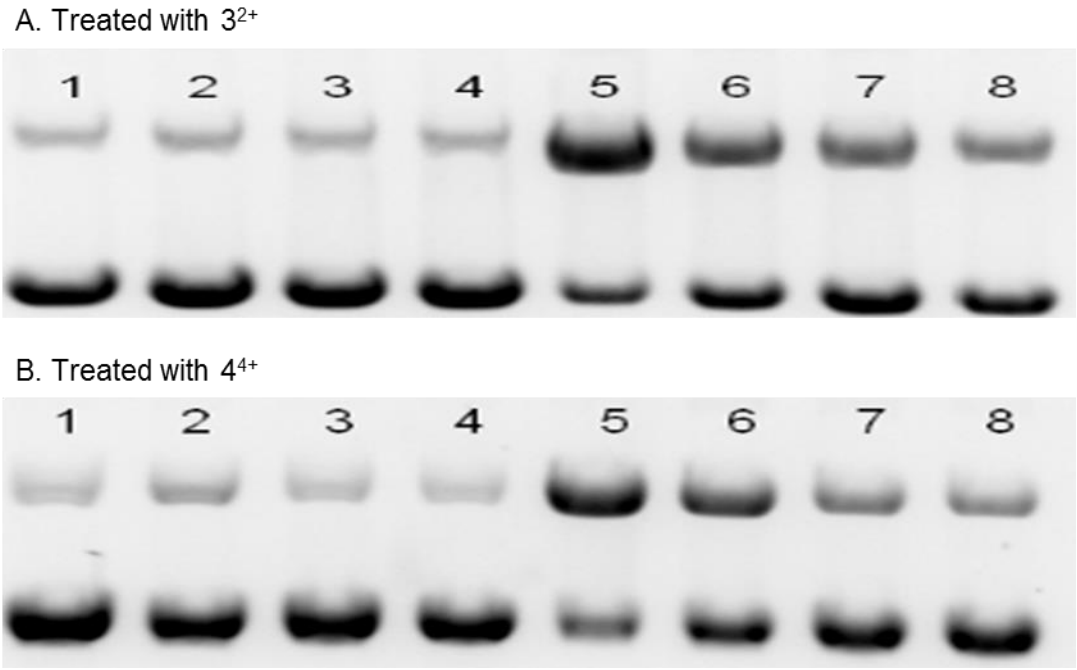

Figure S4. Effect of addition of varying concentrations of sodium formate to the DNA cleavage activity of **3**$^{2+}$ (A. top gel) and **4**$^{4+}$ (B. bottom gel). Agarose gel (1%) stained with ethidium bromide of supercoiled pUC18 DNA (154 µM) cleavage products after incubation at 25 ^{o}C for 48 h with RPC (12.8 µM), GSH (256 µM) in 50 mM Na_3PO_4/10 mM buffer (pH 7.2). Lane 1: DNA control Lane 2: GSH and DNA Lane 3: DNA and RPC Lane 4: sodium formate (6.4 mM) DNA Lane 5: RPC, DNA and GSH Lane 6: RPC, GSH, DNA and sodium formate (2.1 mM) Lane 7: RPC, GSH, DNA and sodium formate (4.2 mM) Lane 8: RPC, GSH, DNA and sodium formate (6.4 mM). All reactions were carried out under aerobic conditions.

A. Treated with 3^{2+}

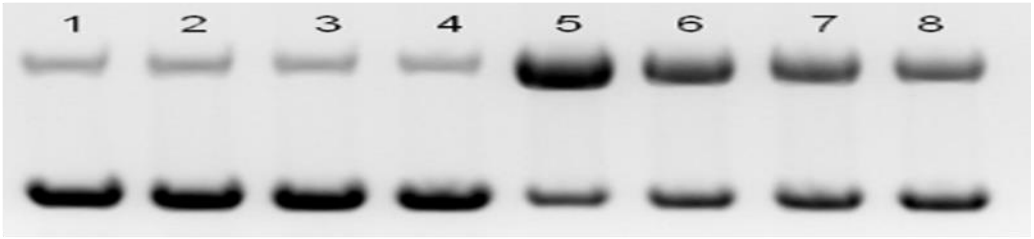

B. Treated with 4^{4+}

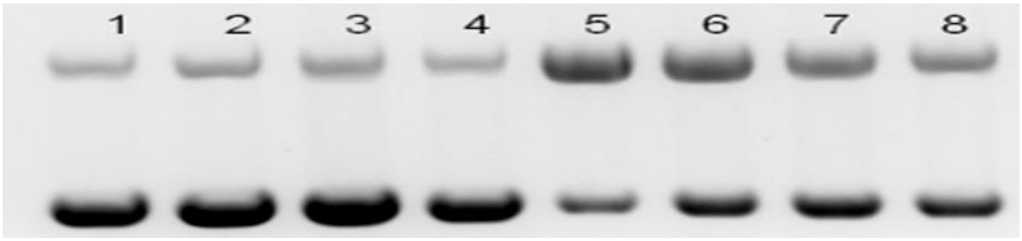

Figure S5. Effect of addition of varying concentrations of mannitol to the DNA cleavage activity of **3**$^{2+}$ (A. top gel) and **4**$^{4+}$ (B. bottom gel). Agarose gel (1%) stained with ethidium bromide of supercoiled pUC18 DNA (154 µM) cleavage products after incubation at 25 ^{o}C for 48 h with RPC (12.8 µM), GSH (256 µM) in 50 mM Na_3PO_4/10 mM buffer (pH 7.2). Lane 1: DNA control Lane 2: GSH and DNA Lane 3: DNA and RPC Lane 4 mannitol (6.4 mM) DNA Lane 5: RPC, DNA and GSH Lane 6: RPC, GSH, DNA and mannitol (2.1 mM) Lane 7: RPC, GSH, DNA and mannitol l (4.2 mM) Lane 8: RPC, GSH, DNA and mannitol (6.4 mM). All reactions were carried out under aerobic conditions.

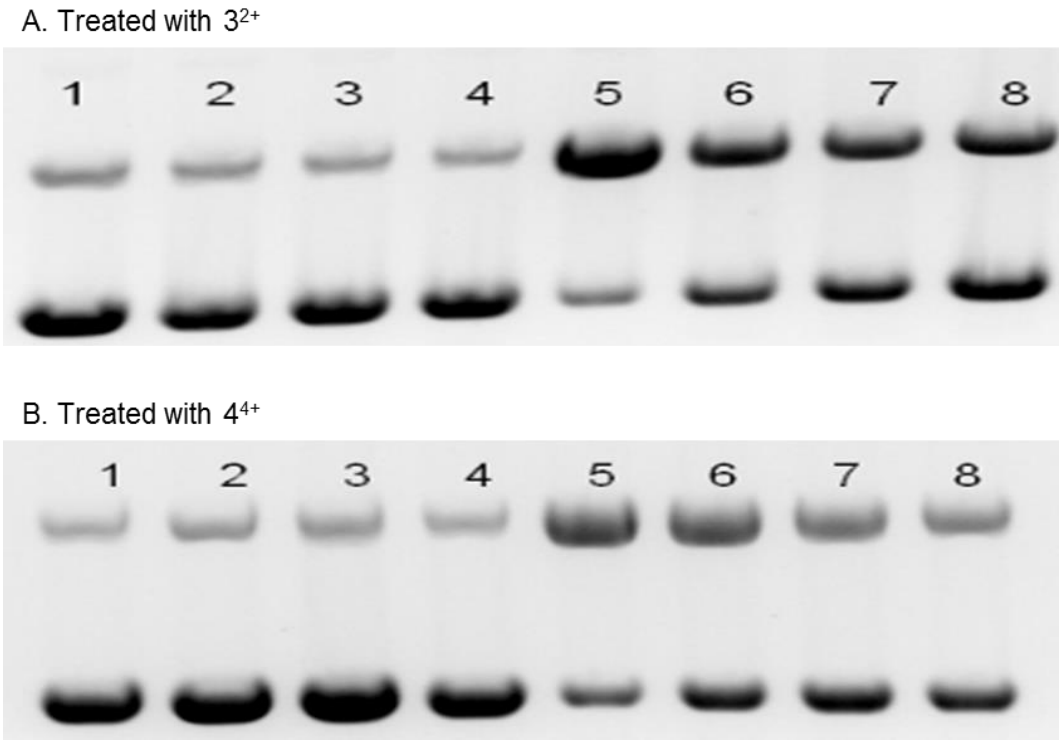

Figure S6. Effect of addition of varying concentrations of ethanol to the DNA cleavage activity of **3**$^{2+}$ (A. top gel) and **4**$^{4+}$ (B. bottom gel). Agarose gel (1%) stained with ethidium bromide of supercoiled pUC18 DNA (154 µM) cleavage products after incubation at 25 ^{o}C for 48 h with RPC (12.8 µM), GSH (256 µM) in 50 mM Na_3PO_4/10 mM buffer (pH 7.2). Lane 1: DNA control Lane 2: GSH and DNA Lane 3: DNA and RPC Lane 4: ethanol (6.4 mM) DNA Lane 5: RPC, DNA and GSH Lane 6: RPC, GSH, DNA and ethanol l (2.1 mM) Lane 7: RPC, GSH, DNA and ethanol (4.2 mM) Lane 8: RPC, GSH, DNA and ethanol (6.4 mM). All reactions were carried out under aerobic conditions.

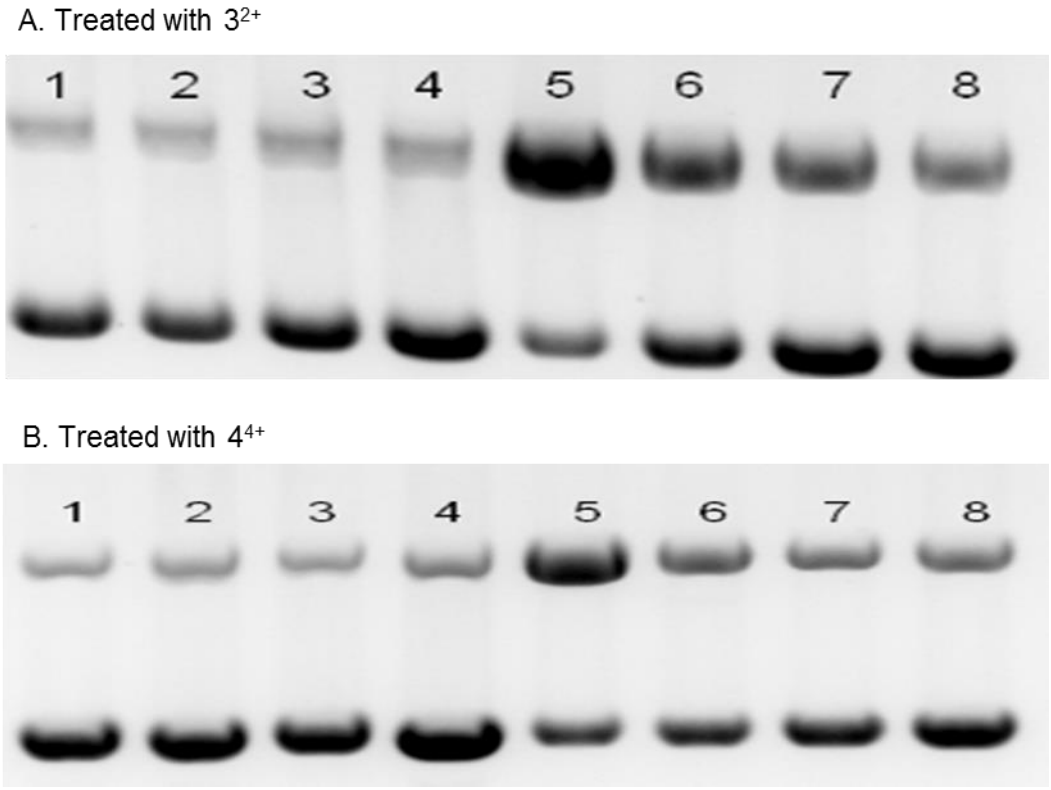

Figure S7. Effect of addition of varying concentrations of DMSO to the DNA cleavage activity of **3**$^{2+}$ (A. top gel) and **4**$^{4+}$ (B. bottom gel). Agarose gel (1%) stained with ethidium bromide of supercoiled pUC18 DNA (154 µM) cleavage products after incubation at 25 ^{o}C for 48 h with RPC (12.8 µM), GSH (256 µM) in 50 mM Na_3PO_4/10 mM buffer (pH 7.2). Lane 1: DNA control Lane 2: GSH and DNA Lane 3: DNA and RPC Lane 4: DMSO (6.4 mM) DNA Lane 5: RPC, DNA and GSH Lane 6: RPC, GSH, DNA and DMSO (2.1 mM) Lane 7: RPC, GSH, DNA and DMSO (4.2 mM) Lane 8: RPC, GSH, DNA and DMSO (6.4 mM). All reactions were carried out under aerobic conditions.

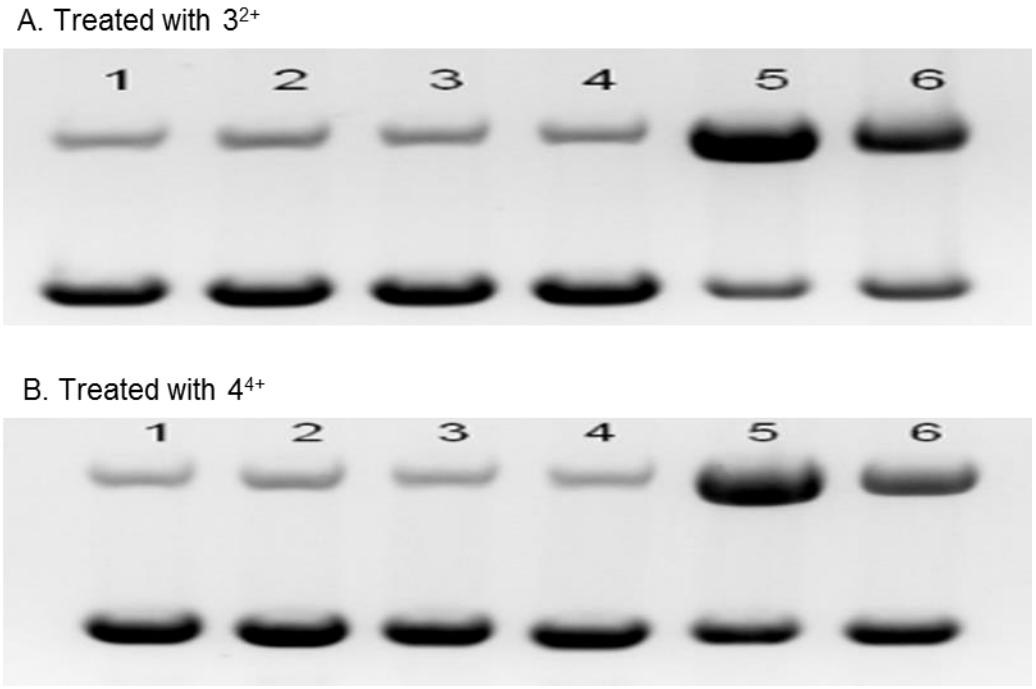

Figure S8. Effect of addition of varying concentrations of SOD to the DNA cleavage activity of **3**$^{2+}$ (A. top gel) and **4**$^{4+}$ (B. bottom gel). Agarose gel (1%) stained with ethidium bromide of supercoiled pUC18 DNA (154 µM) cleavage products after incubation at 25 ^{o}C for 48 h with RPC (12.8 µM), GSH (25 6 µM) in 50 mM Na_3PO_4/10 mM buffer (pH 7.2). Lane 1: DNA control Lane 2: GSH and DNA Lane 3: DNA and RPC Lane 4: SOD (15 µg/mL) DNA Lane 5: RPC, DNA and GSH Lane 6: RPC, GSH, DNA and SOD (15 µg/mL). All reactions were carried out under aerobic conditions.

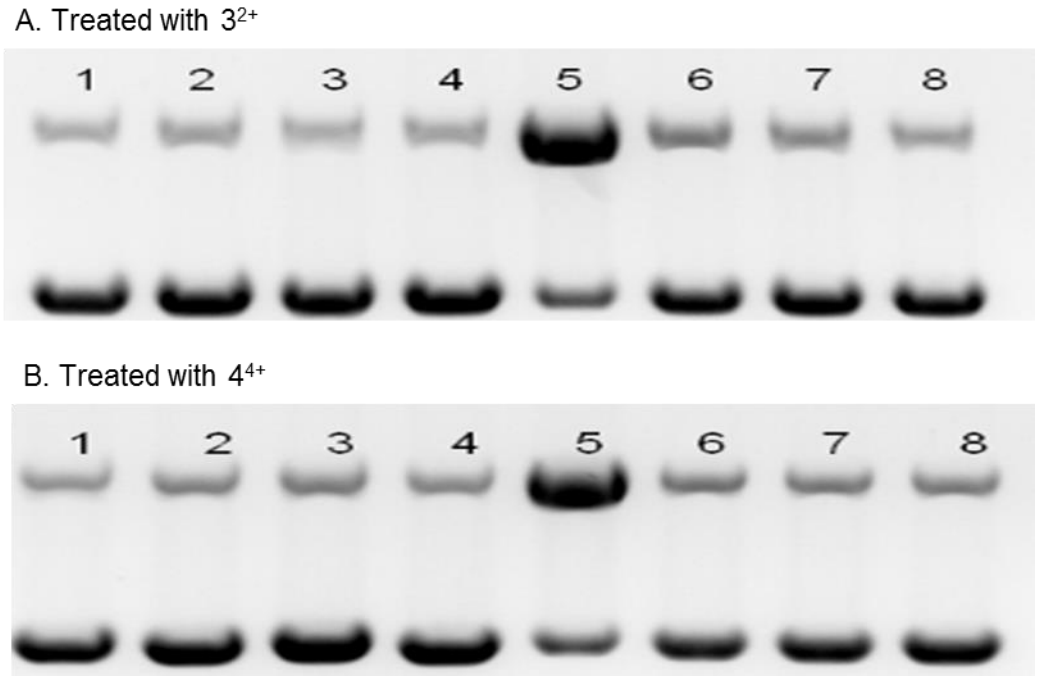

Figure S9. Effect of addition of varying concentrations of sodium pyruvate to the DNA cleavage activity of **3**$^{2+}$ (A. top gel) and **4**$^{4+}$ (B. bottom gel). Agarose gel (1%) stained with ethidium bromide of supercoiled pUC18 DNA (154 µM) cleavage products after incubation at 25 ^{o}C for 48 h with RPC (12.8 µM), GSH (256 µM) in 50 mM Na_3PO_4/10 mM buffer (pH 7.2). Lane 1: DNA control Lane 2: GSH and DNA Lane 3: DNA and RPC Lane 4: sodium pyruvate (6.4 mM) DNA Lane 5: RPC, DNA and GSH Lane 6: RPC, GSH, DNA and sodium pyruvate (2.1 mM) Lane 7: RPC, GSH, DNA and sodium pyruvate (4.2 mM) Lane 8: RPC, GSH, DNA and sodium pyruvate (6.4 mM). All reactions were carried out under aerobic conditions.

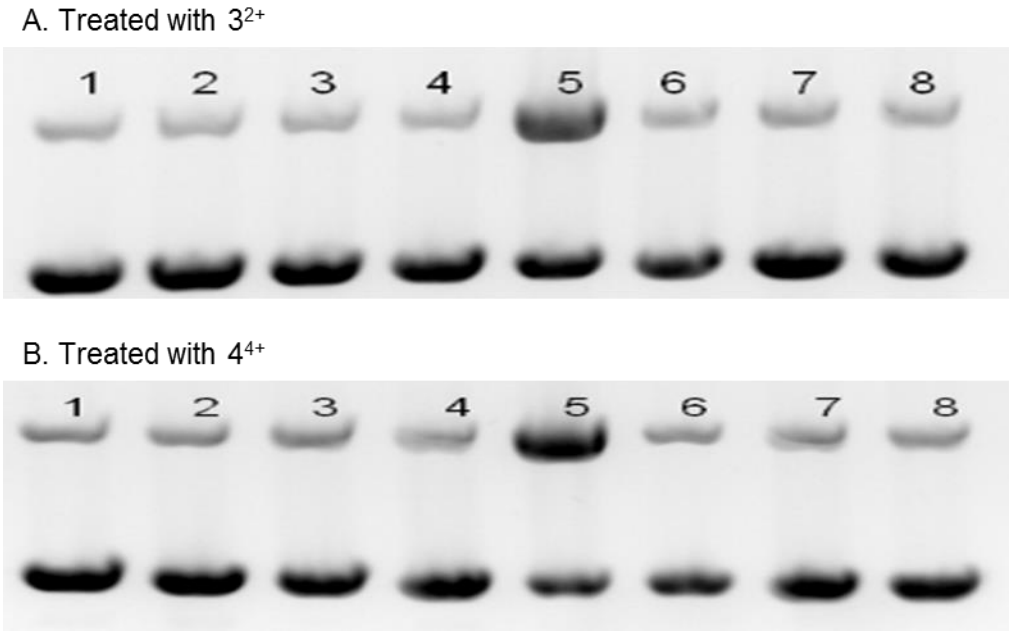

Figure S10. Effect of addition of varying concentrations of deferoxamine mesylate salt (DEF) to the DNA cleavage activity of **3**$^{2+}$ (A. top gel) and **4**$^{4+}$ (B. bottom gel). Agarose gel (1%) stained with ethidium bromide of supercoiled pUC18 DNA (154 µM) cleavage products after incubation at 25 ^{o}C for 48 h with RPC (12.8 µM), GSH (256 µM) in 50 mM Na_3PO_4/10 mM buffer (pH 7.2). Lane 1: DNA control Lane 2: GSH and DNA Lane 3: DNA and RPC Lane 4: DEF (6.4 mM) DNA Lane 5: RPC, DNA and GSH Lane 6: RPC, GSH, DNA and DEF (2.1 mM) Lane 7: RPC, GSH, DNA and DEF (4.2 mM) Lane 8: RPC, GSH, DNA and DEF (6.4 mM). All reactions were carried out under aerobic conditions.

2.5.4 DNA Scission Experiment with HPLC Product Analysis

Experiments were conducted under the following conditions, (45.5 mL) 700 μM ctDNA, (4.1 mL) 58.3 μM (**4**$^{4+}$), (19.9 mL) 5.8 mM GSH, (30.5 mL) 50 mM phosphate, 10 mM NaCl Buffer at pH 7.4 digested at room temperature in air overnight , then heated at 90 °C for 1hr in a GC oven. The reaction was quenched with ice bath (dry ice/acetone), extracted with 20 mL dichloromethane (DCM) 3x, dried with magnesium sulfate ($MgSO_4$) and concentrated. Samples were resuspended in pure acetonitrile (MeCN) for HPLC analysis using an Agilent Infinity 1200 series HPLC.

The mobile phase of for HPLC was 0.1 TFA/MeCN 90/10, Flow Rate: 0.1mL/min ,Injection Vol: 10 μL, Stationary Phase: Zorbax Eclipse XDB-C18 4.6x150 column. The same method was conducted for **3**$^{2+}$.

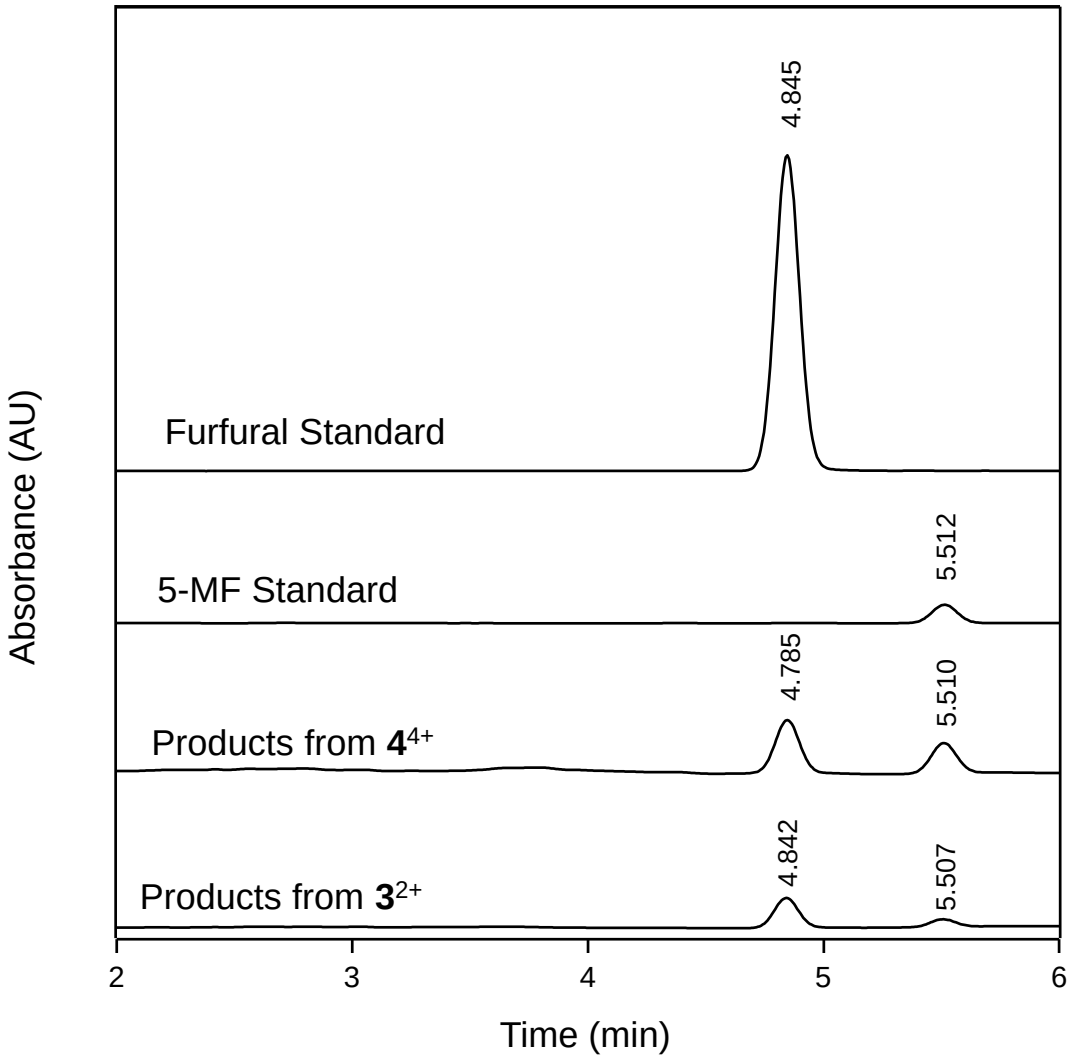

Figure S11 HPLC analysis of 5-MF and furfural at 280 nm, analyzed on a Agilent 1200 series with a mobile phase of 0.1 TFA/MeCN 90/10, Flow Rate: 0.1mL/min ,Injection Vol: 10 µL, Stationary Phase: Zorbax Eclipse XDB-C18 4.6x150 column.

Table S1 First reduction potential for $\mathbf{1}^{2+}$ – $\mathbf{8}^{4+}$ as obtained in acetonitrile with references

Compound	Solvent	Couple	Potential (V) vs NHE*	Ref
$\mathbf{1}^{2+}$ $[Ru(phen)_3]^{2+}$	MeCN	$1^{2+}/^{+}$	-1.15 (1 e-)	164-168
$\mathbf{2}^{2+}$ $[Ru(byp)_3]^{2+}$	MeCN	$2^{2+}/^{+}$	-1.11 (1 e-)	164,165,168
$\mathbf{3}^{2+}$ $[(phen)_2Ru(tatpp)]^{2+}$	MeCN	$3^{2+}/3^{+}$	-0.11 (1 e-)	138,169
	MeCN	$3^{+}/3^{0}$	-0.65 (1 e-)	138,169
$\mathbf{4}^{4+}$ $[(phen)_2Ru(tatpp)Ru(phen)_2]4^{+}$	MeCN	$4^{4+}/4^{3+}$	-0.02 (1 e-)	137,167
	MeCN	$4^{3+}/4^{2+}$	-0.51 (1 e-)	137,167
$\mathbf{5}^{2+}$ $[(phen)_2Ru(tatpq)Ru(phen)_2]^{4+}$	MeCN	$5^{4+}/5^{3+}$	0.04 (1e-)	169
$\mathbf{6}^{2+}$ $[(phen)_2Ru(dppz)]^{2+}$	MeCN	$6^{2+}/^{+}$	-0.73 (1 e-)	170,171
$\mathbf{7}^{2+}$ $[(phen)_2Ru(tpphz)]^{2+}$	MeCN	$7^{2+}/^{+}$	-0.76 (1 e-)	99,171,172
$\mathbf{8}^{4+}$ $[(phen)_2Ru(tpphz)Ru(phen)_2]^{4+}$	MeCN	$8^{4+}/3^{+}$	-0.54 (1 e-)	172

*All reduction potentials have been converted to NHE if not already done so in literature.

Chapter 3

INTRODUCTION TO CHIRAL SEPARATIONS

3.1 Perspective

Chiral separation is essential for the discovery and development of therapeutics, with enantiomeric forms often possessing different biological effects. Due to the importance of chirality in biological responses, government and industries often require chiral compounds in their enantiomeric pure form.[173] During the drug development process, it is not only essential but also required by the FDA to fully elucidate enantiomeric differences regarding efficacy, toxicity, and biological activity.[174] There are two methods to achieve enantiomeric purity of a compound when considering a synthetic route. Once is by an asymmetric synthetic approach yielding only one of the enantiomers. The second is racemic synthesis followed by separation of the racemates. There are many methods and factors to consider to achieve enantiomeric purity. For small scale testing of the enantiomers to be used in *in vivo* and *in vitro* studies, purification by HPLC provides an effective way to not only ensure purification but also measure any potential enantiomeric excess.[173]

Due to the robust nature, distinctive electrochemical and photophysical characteristics of ruthenium(II) polypyridyl complexes a wide variety of RPCs have been synthesized and investigated for a multitude of applications ranging from energy to medicinal uses. Many RPCs are known to have specific interactions with DNA and have been widely used for cellular imaging and therapeutics, as they are known to have specific interactions with DNA.[13-15,50] In

addition to medicinal investigations and uses, ruthenium(II) complexes are effective catalysts for organic synthesis and dye sensitizers for solar cells.[16-19] Ruthenium(II) polypyridyl complexes exhibit axial chirality and the right- and left-handed configurations of the octahedral complexes are referred to as Δ (delta)- and Λ (lambda)-enantiomers respectively. It is known the enantiomers of ruthenium(II) complexes exhibit very different biological activities when used as inhibitors of enzyme activity, DNA intercalating agents, and stabilizers of G-Quadruplex DNA.[20-22] When RPCs are used as a catalyst, enantiomers of ruthenium(II) complexes dramatically influence the stereochemistry of chiral products.[23] Therefore, the need for analytical methods by which ruthenium(II) polypyridyl complex enantiomers can be separated, evaluated, and purified cannot be overstated.

The separation of geometric isomers, diastereomers, and enantiomers of several ruthenium complexes have been achieved by chromatographic methods and capillary electrophoresis by the Armstrong Group using different chiral selectors.[175-179] Capillary electrophoresis is not suitable for preparative-scale separations and, as such, high-performance liquid chromatography (HPLC) with chiral stationary phases (CSPs) has proven to be the best way to separate enantiomers of organometallic compounds due to the technique's broad selectivity, high efficiency, and ability to transition to preparative-scales.[179] For example, the Armstrong Group has shown enantiomeric separation of ruthenium polypyridyl complexes has been obtained with macrocyclic glycopeptide CSPs

and cyclodextrin (CD) CSPs and cyclofructan (CF), with cyclofructan yielding more favorable results.[178,179]

As seen in Figure 3.1, cyclofructans (CFs) are naturally occurring chiral crown ethers which consist of β-(2-1) linked D-fructofuranose units and are structural isomers of CDs. The Armstrong Group developed the R-naphthylethyl-carbamate CF6 (LARIHC CF6-RN) bonded chiral stationary phase for HPLC along with several other derivatized CF6 phases.[179] The LARIHC CF6-RN showed unique selectivity and broad applicability for amine-containing racemates and the greatest selectivity between RPCs enantiomers. Previous studies showed the R-naphthylethyl functionalized CF6 CSP proved more suitable for the enantiomeric separation of binaphthyl catalysts when compared to the R-naphthylethyl functionalized CD CSP.[180] Therefore, for the purposes of this work we chose the CF6-RN for all separation studies and semi-preparative optimizations.

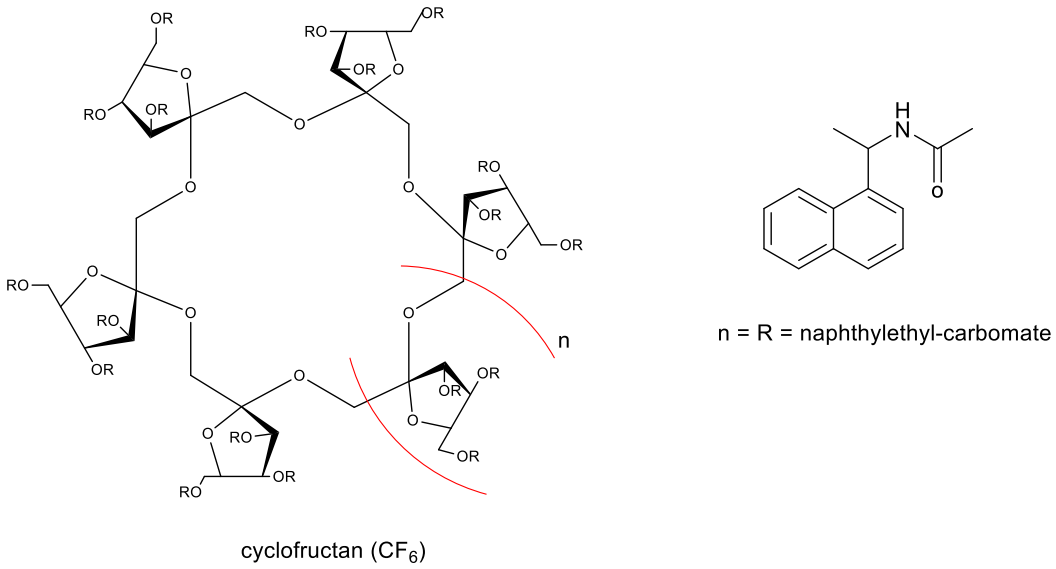

Figure 3.1 Structure of the CF6-RN bonded stationary phase for the LARIHC CF6-RN column.

Given the stringent requirements implemented by the FDA in 1992[174] it is vital that enantiomeric testing for any drug intended for medicinal use be of the utmost purity. In this work, we have focused on the enantioseparation of $[Ru(phen)_2phendione]^{2+}$ as this is a key synthetic intermediate for numerous RPC's, including $[(phen)_2Ru(tatpp)]^{2+}$ ($\mathbf{3}^{2+}$) and $[(phen)_2Ru(tatpp)Ru(phen)_2]^{4+}$ ($\mathbf{4}^{4+}$) (figure 3.3). The enantiomers of $[Ru(phen)_2phendione]^{2+}$ are key synthetic intermediates for the preparation of a large variety of RPCs. The quinone function offers a C2 symmetric addition point to initiate pyrazines, imidazoles Δ or λ enantiomer could be prepared in quantity by HPLC, then the subsequent preparation of enantiopure derivatives would be trivial. Because of this, we focused on developing analytical and analytical and prep scale conditions for the

separation of racemic [Ru(phen)$_2$phendione]$^{2+}$ using cyclofructan HPLC chiral stationary phases building off the work of Armstrong et al.

By purifying the enantiomers of [Ru(phen)$_2$phendione]$^{2+}$ this will allow asymmetric synthesis of [Ru(phen)$_2$phendione]$^{2+}$ to yield the desired enantiomers of **3**$^{2+}$ and **4**$^{4+}$ (Figure 3.3) avoiding the time consuming process of asymmetric synthesis to yield enantiopure products.

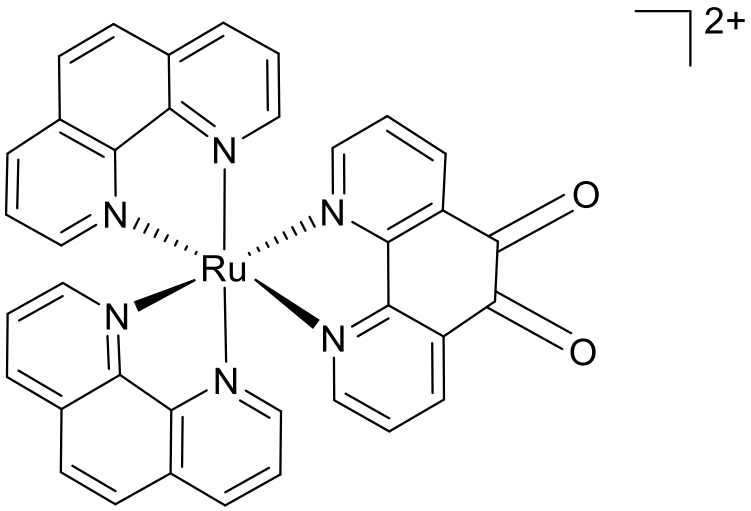

Figure 3.2 Structure of [Ru(phen)$_2$phendione]$^{2+}$

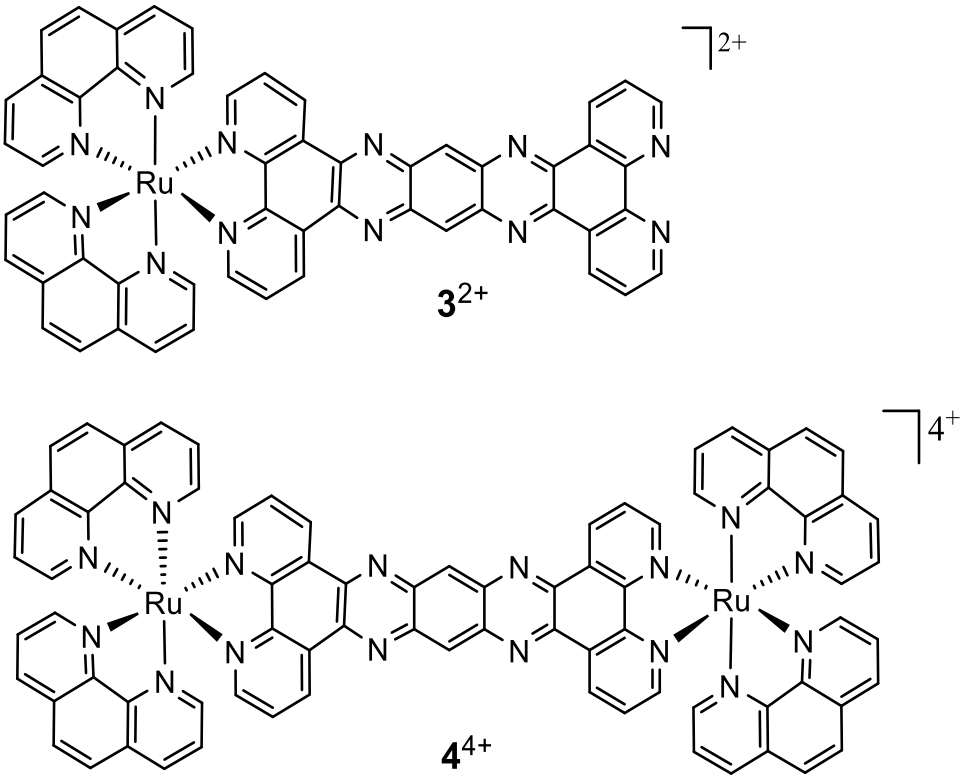

Figure 3.3 Structure of $\mathbf{3}^{2+}$ and $\mathbf{4}^{4+}$

In addition to the semi-preparative development for enantiomeric purification of $[Ru(phen)_2phendione]^{2+}$, in a collaborative work with Dr. Sherri McFarland of the University of North Carolina at Greensboro we developed a method for the analytical enantiomeric separation of 6 new derivatives of $[Ru(phen)_2phendione]^{2+}$ synthesized by her group (shown in figure 3.4). Figure 3.5 denotes the abbreviated nomenclature for ligands of the $[Ru(phen)_2phendione]^{2+}$ derivatives. From this work these compounds will undergo enantiomeric purification by semi-preparative for further analysis as potential therapeutics in the ongoing fight treat cancer.

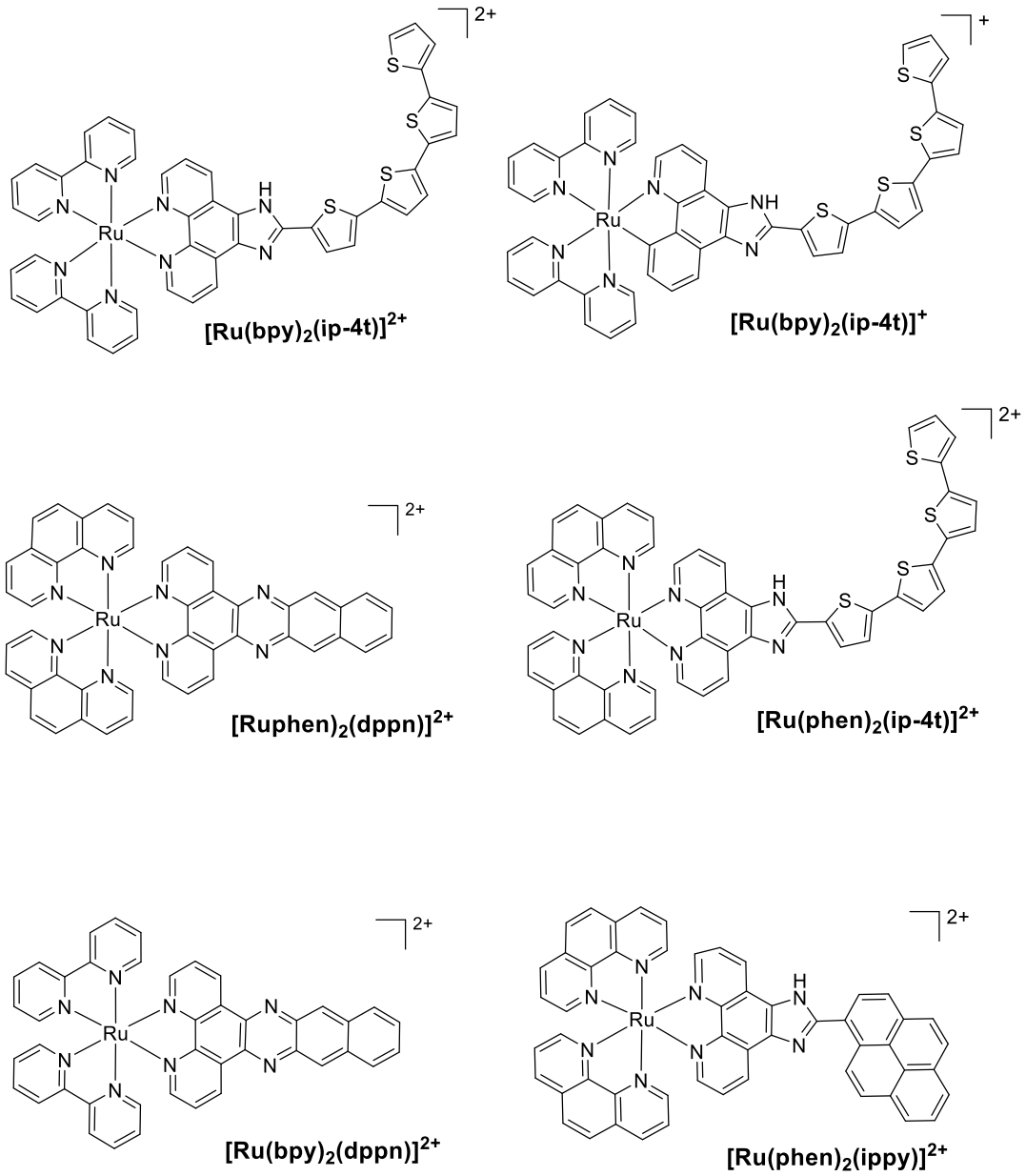

Figure 3.4 RPCs from the McFarland Group

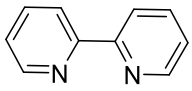

2,2'-bipyridine = bpy = a

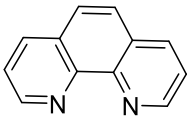

1,10-phenanthroline = phen = b

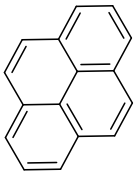

pyrene = py

thiophene = t

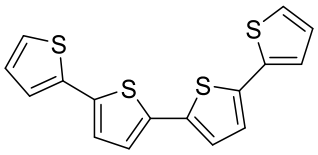

2,2':5',2'':5'',2'''-quaterthiophene =4t

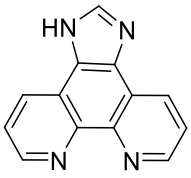

1*H*-imidazo[4,5-*f*][1,10]phenanthroline = ip

Figure 3.5 Ligands and nomenclature

3.2 Experimental

3.2.1 Materials and Reagents

[Ru(phen)$_2$phendione] $(PF_6)_2$ $5H_2O$ was synthesized according to literature. [181] RPC's provided by the McFarland group $[Ru(phen)_2(ippy)]^{2+}$,$[Ru(phen)_2(dppn)]^{2+}$,$[Ru(byp)_2(dppn)]^{2+}$, $[Ru(byp)_2(ip\text{-}4t)]^{+}$, and $[Ru(byp)_2(ip\text{-}4t)]^{2+}$, were synthesized according to literature.[182-184] .Reagents and solvents for HPLC analysis, methanol, acetonitrile and ammonium nitrate (NH_4NO_3) were purchased from Sigma and VWR respectively. The analytical LARIHC CF6-RN (4.6 x 25 mm) and the semi-prep LARIHC CF6-RN (250 x 21.2 mm) were purchased from AZYP Separations and Analytics, LLC.

3.2.2 Instrumentation

Analytical HPLC analysis of [Ru(phen)$_2$phendione] $(PF_6)_2$ was carried out on a Shimadzu UFLC XR Series, LC-20AD XR Pump, SIL-20AC XR Auto sampler, with a SPD-M20A Diode Array Detector. Lab Solutions software was used to derive and process the chromatograph and chromatograms respectively. The flow cell temperature was 40℃. The column oven was room temperature. The wavelength was set at 254 nm. The injection volumes varied by study from 1 to 20 uL. The flowrate was 1 mL/min. The Mobile phase ratios of methanol to acetonitrile varied per study. However, the concentration of NH_4NO_3 remained constant at 0.025 M. The concentration of NH_4NO_3 was relevant to methanol since it is not soluble in acetonitrile. A separate pump was used to for

the methanol containing NH_4NO_3 while the other pump contained only acetonitrile. Therefore the ratio of the mobile phase was binary but at an isocratic total flow of 1 mL/min.

Prep-Scale HPLC analysis of [Ru(phen)$_2$phendione] $(PF_6)_2$ was carried out on a Shimadzu Prep LC, LC-20AP Pump, SIL-10AP Auto sampler, with a SPD-20AV UV-Vis Detector. Lab Solutions software was used to derive and process the chromatograph and chromatograms respectively. The flow cell temperature was 40℃. The column oven was room temperature. The wavelength was set at 254 nm. The injection volumes varied by study from 1000 to 3000 uL. The flowrate was 10 mL/min. The Mobile phase ratios of methanol to acetonitrile was 75:25. The concentration of NH_4NO_3 remained constant at 0.025 M. The concentration of NH_4NO_3 was relevant to methanol since it is not soluble in acetonitrile. A separate pump was used to for the methanol containing NH_4NO_3 while the other pump contained only acetonitrile. Therefore the ratio of the mobile phase was binary but at an isocratic total flow of 10 mL/min.

3.2.3 Sample Prep

Samples for analytical studies were dissolved in acetonitrile and were diluted down from 1 mg/mL to various concentrations per study. All mobile phases were degassed prior to use. Ammonium nitrate was dissolved in methanol at a concentration of 0.025 M. For analytical studies, LC grade solvents were used. For pre-scale purification, reagent grade solvents were used.

3.3 Results and discussion

3.3.1 Results for analytical optimization of selectivity for [Ru(phen)$_2$phendione] (PF$_6$)$_2$

In an effort to maximize the greatest selectivity (α) between enantiomers we investigated various mobile phase ratios and salt concentrations. As seen in Figure 3.6 and 3.7 the change in salt concentrations had no significant effect on selectivity.

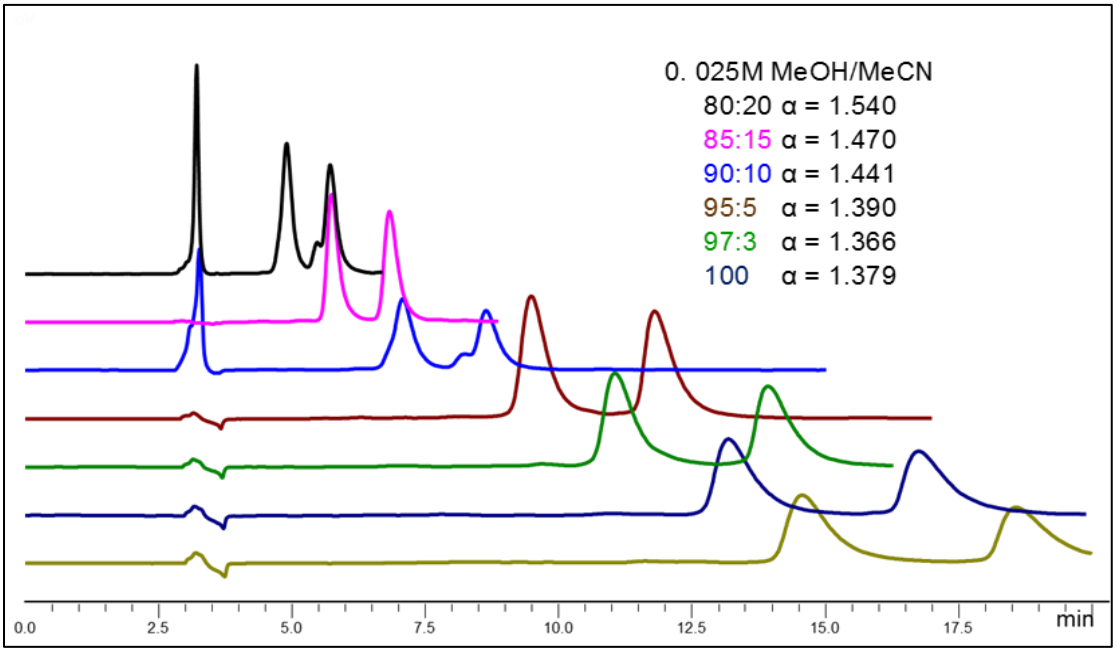

Figure 3.6 LC chromatograph of [Ru(phen)$_2$phendione] $(PF_6)_2^+$ at various mobile phase ratios with a salt concentration of 0.025 M NH_4NO_3.

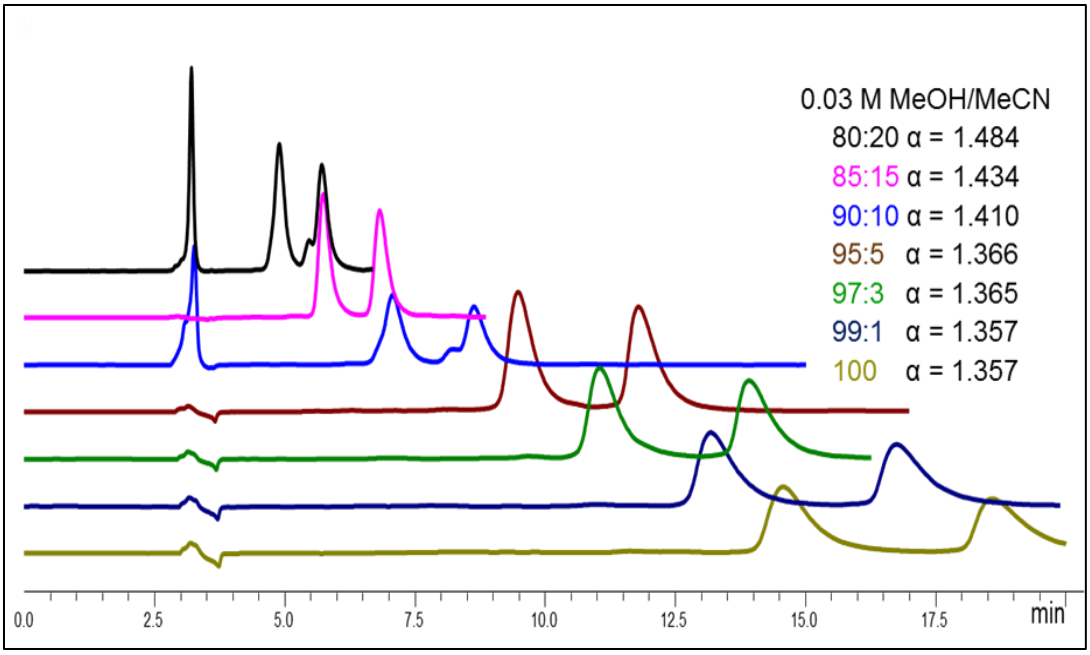

Figure 3.7 LC chromatograph of [Ru(phen)$_2$phendione] $(PF_6)_2$ at various mobile phase ratios with a salt concentration of 0.03 M NH_4NO_3.

In figure 3.7 it is clearly shown that manipulations of the mobile phase ratios of methanol to acetonitrile had a significant impact on the retention factor (k') of the enantiomers and very little effect on changes in resolution (R_s) and selectivity. . Interestingly, the retention factor (k_2') for the lambda enantiomer was consistently greater with every ratio investigated. However, since the selectivity remained relatively consistent with each mobile phase ratio we were able to focus optimization on retention time (t_R). For the analytical study we found the optimal time was with a ratio of 75:25 MeOH/MeCN with a total run time just under 8 minutes. Although the data for the optimal ratio of 75:25 MeOH/MeCN is

not shown in figures 3.6 or 3.7, it is shown in figure 3.8 and in the prep scale studies. From the data shown in figure 3.8 it is much easier to see the selectivity for [Ru(phen)$_2$phendione] $(PF_6)_2$ remains relatively consistent with a slight decrease as the amount of methanol increases. Not only is this not optimal for prep scale enantiomeric purification we see the retention time increases significantly as the methanol ratio increases. As the acetonitrile ratio increases above 75:25 the retention factor and resolution start to decrease. These are not optimal conditions either. Therefore we determined 75:25 methanol/acetonitrile to be the optimal mobile phase for analytical enantiomeric separation of [Ru(phen)$_2$phendione] $(PF_6)_2$

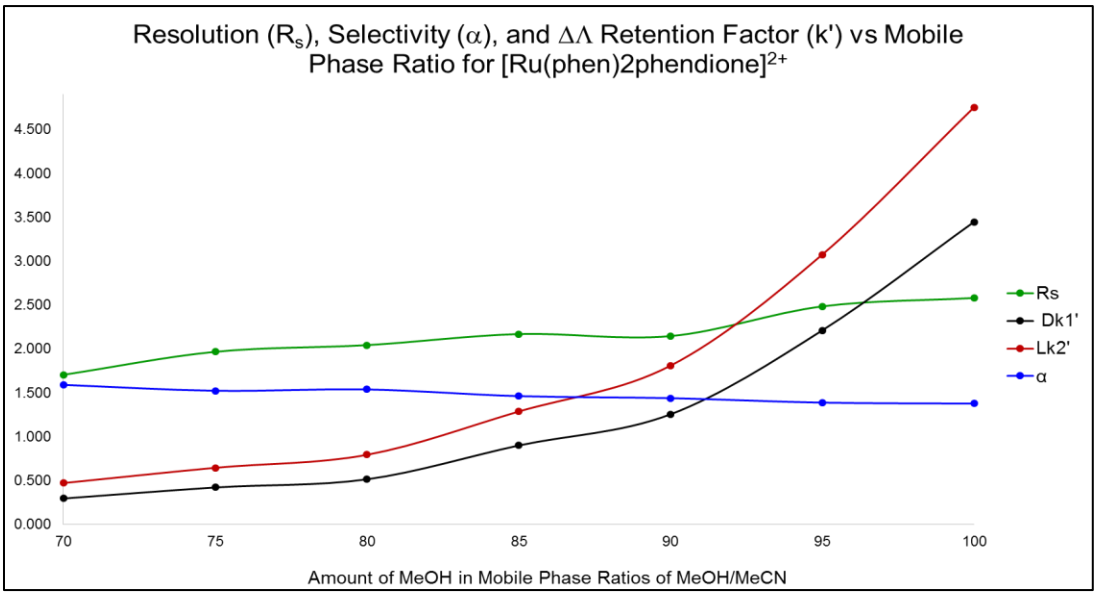

Figure 3.8 Graph of Rs, α, k_1',k_2' vs mobile phase ratios of MeOH(0.025 M NH_4NO_3)/MeCN ranging from 70:30 to 100% MeOH.

3.3.2 Results for prep-scale optimization of selectivity for [Ru(phen)$_2$phendione] (PF_6)$_2$

From the information obtained in the analytical studies we determined the optimal conditions for prep-scale enantiomeric purification was 75:25 MeOH (0.025 M NH_4N0_3)/MeCN. Attempts were made to do a loading study on the analytical column to determine the maximum amount (mg of RPC) the semi-prep scale column could purify per run. However, due to pressure limitations of the pumps, solubility, and column limitations the maximum amount we could achieve was 50 uL injection of sample containing 10 mg/mL (0.50 mg) of the RPC. As seen in figure 3.9 resolution of the enantiomers decreased significantly.

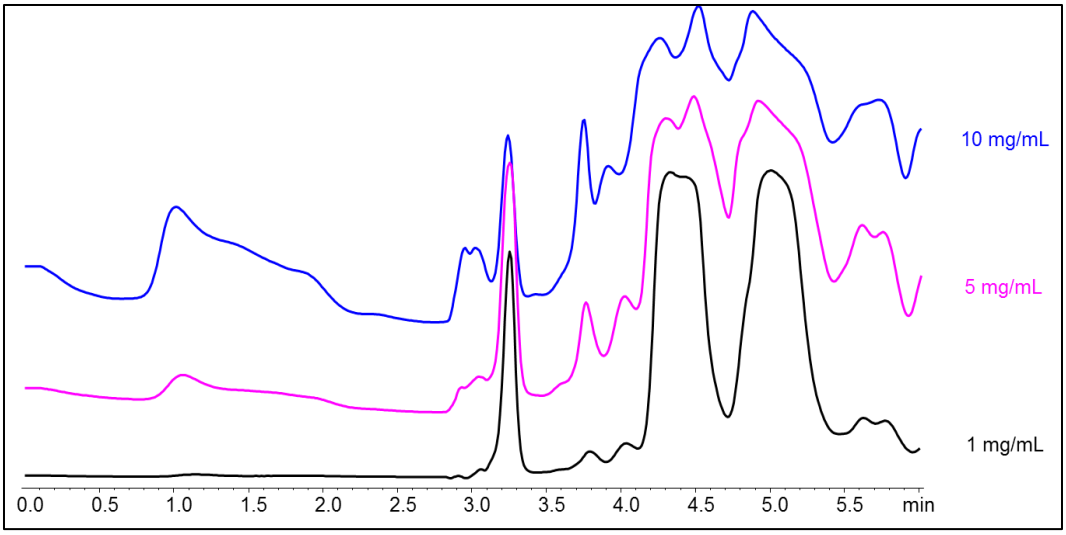

Figure 3.9 50 uL injection of sample containing 1 (0.05 mg), 5 (0.025 mg), and 10 mg/mL (0.50 mg) of [Ru(phen)$_2$phendione] $(PF_6)_2$ for loading study on analytical column LARIHC-CF6-RN

In theory, a loading study should be done on an analytical column. Then applying that information to a scaling factor should determine the maximum the prep-scale column can achieve. This is true and applies when there is not an attempt to overload the column with sample. As seen in figure 3.10 the prep-scale column was able to resolve 10 mg/mL of sample with ease.

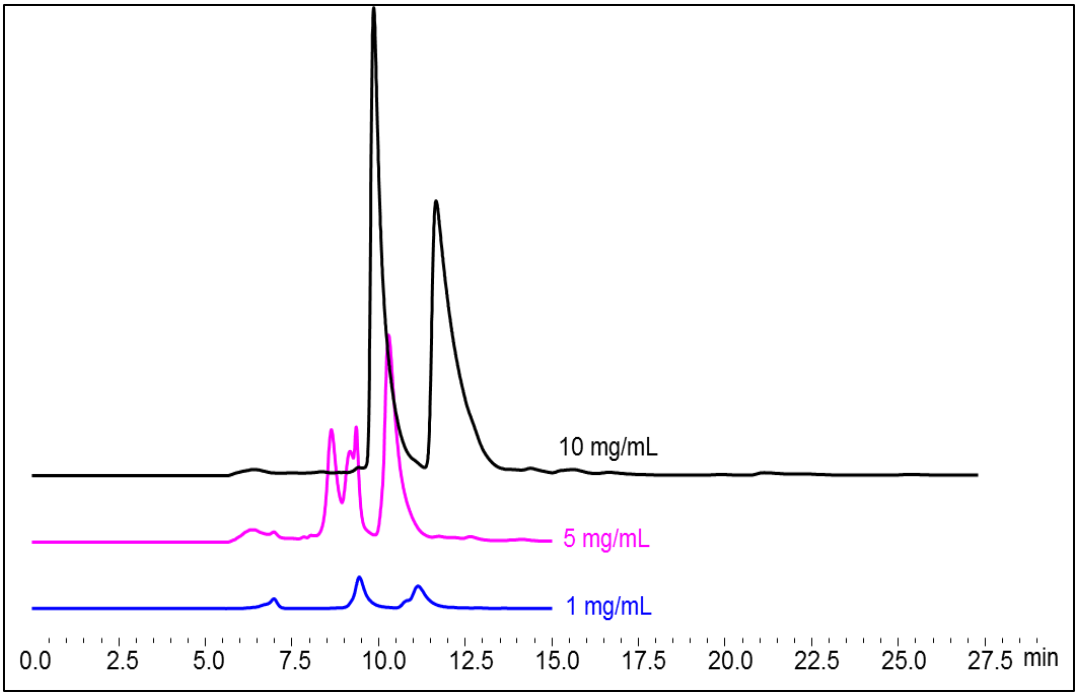

Figure 3.10 1000 uL injection of sample containing 1, 5, and 10 mg/mL of [Ru(phen)$_2$phendione](PF$_6$)$_2$ for loading study on semi-prep column LARIHC-CF6-RN

When we attempted 20 mg/mL of sample overloading began (data not shown). Ultimately, it was found the column was capable of resolving the enantiomeric peaks at a maximum load/run of ~ 85 mg/2mL

Meaning a total of 170 mg of the RPC was separated and purified in one run with a total run time ~12 minutes and total amount of 120 mL of mobile phase used. In figure 3.11 below it shows the prep scale data as well as the analytical data for the collected fractions.

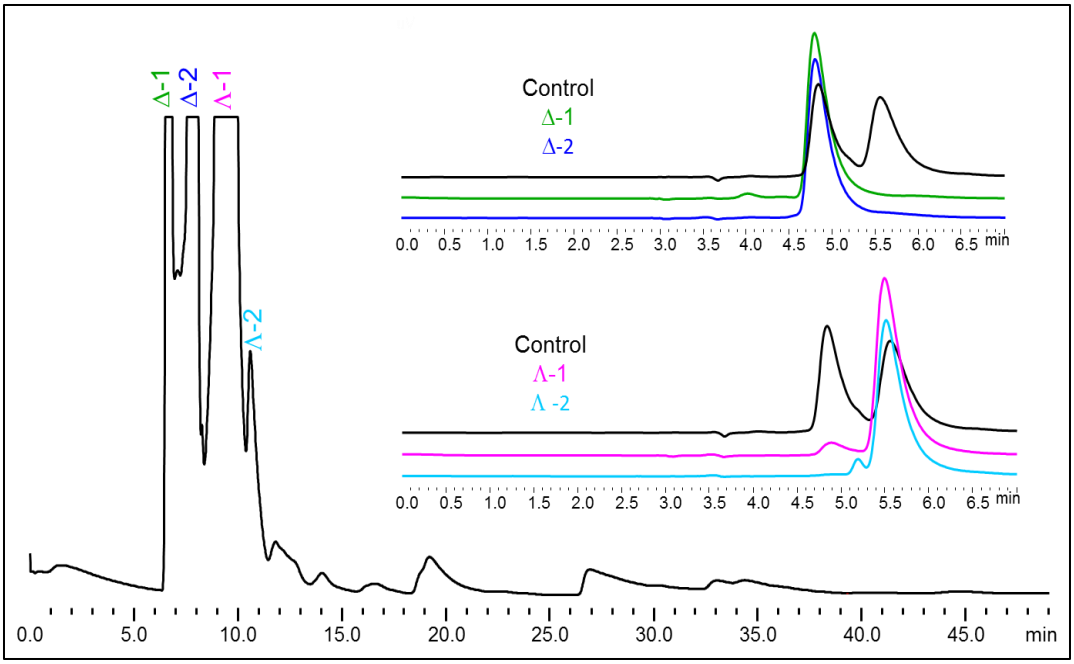

Figure 3.11 2000 uL injection of sample containing 85 mg/mL of [Ru(phen)$_2$phendione] $(PF_6)_2$ for loading study on semi-prep column LARIHC-CF6-RN with analytical analysis of fraction collections as indicated.

Considering the cost of LC grade solvents and the need for optimal chromatograph resolution, we used reagent grade solvents. Two more attempts were made to test the limits of the column with a total amount of sample injected at 255 mg and 420 mg respectively. Although the data for the attempt at 420 mg/run indicated a separation it was clear the peaks that appeared separated contained significant amounts of both enantiomers as seen in figure 3.11. From a comparison of the data in Figure 3.11 and 3.12 we found amounts greater than 150 mg per run does not yield enantiopure separation for LC purification.

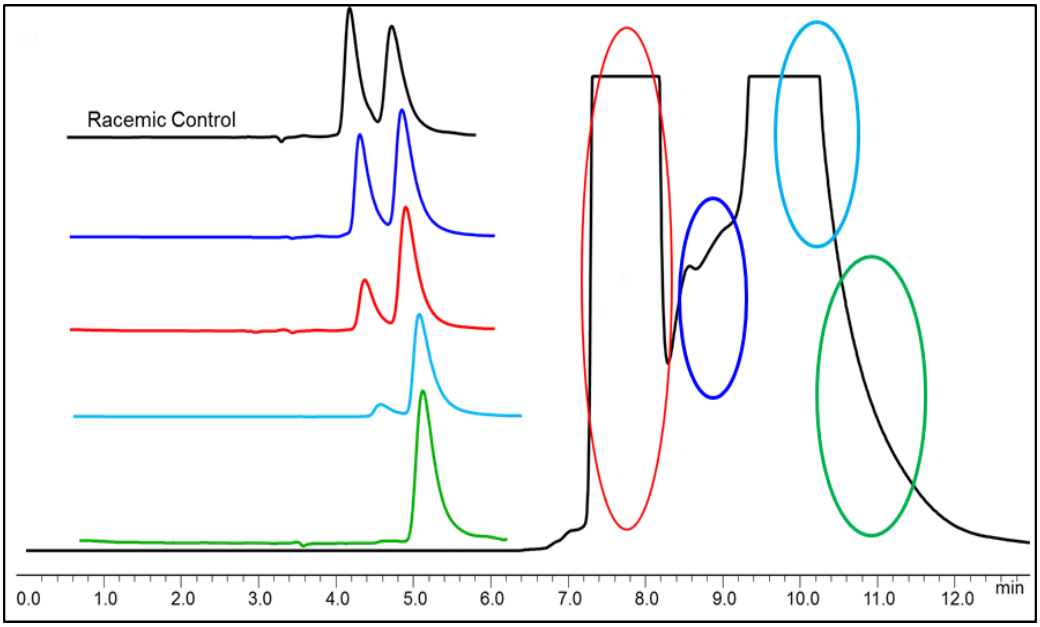

Figure 3.12 Semi-prep scale enantiomeric purification attempt at 420 mg/run of [Ru(phen)$_2$phendione] $(PF_6)_2$. The stacked data is the comparison of the respective collections compared to the racemic control run on an analytical scale.

In summary we found the data to show the optimal method for prep-scale enantiomeric purification of [Ru(phen)$_2$phendione] $(PF_6)_2$ to be 75:25 MeOH/MeCN with 0.025 M NH4NO3 at ~75 mg/ mL (150 mg/run) injection with a flow rate of 10 mL/min. The ability to purify this amount of the enantiomers for this RPC per run within a 12 min period will prove very useful for future synthetic needs and for enantiopure therapeutic testing and asymmetric synthesis of RPCs.

3.3.3 Results for analytical method development of Ru(II) complexes from the McFarland Group.

.

Given the success we have shown with LARIHC-CF6 RN column we choose this column to separate the 6 new compounds. We also started with a similar method as was used for [Ru(phen)$_2$phendione] (PF_6)$_2$. As seen in figures 3.13-3.15 the complexes had varying selectivity and retention times depending on the charge and π bonds in the complex. When comparing the results between the cyclometalated Rua$_2$pb16 (+ charge) to 16a with (2^+ charge) it is clear the reduction in charge decreases the overall run time of the racemic mixture is considerable as the ratio of methanol increases. However, when comparing 16a to 16b it is seen the more π-π interactions increase the greater the selectivity as methanol increases. Although selectivity between complexes varied, selectivity for each compound analyzed at different mobile phase ratios remained relatively consistent.

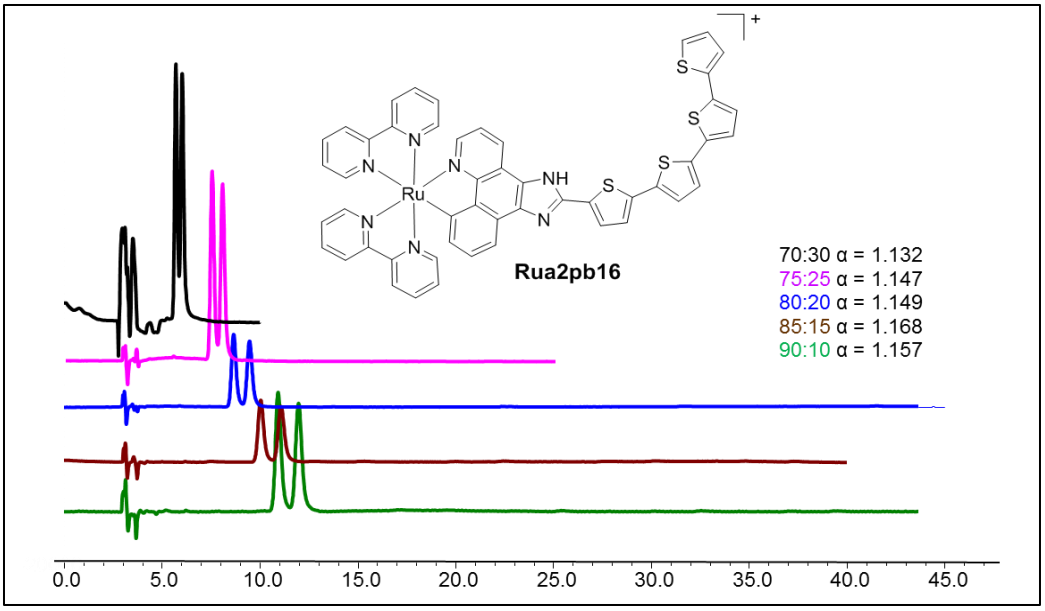

Figure 3.13 [Ru(bpy)2(ip-4t)] (PF_6) optimization study

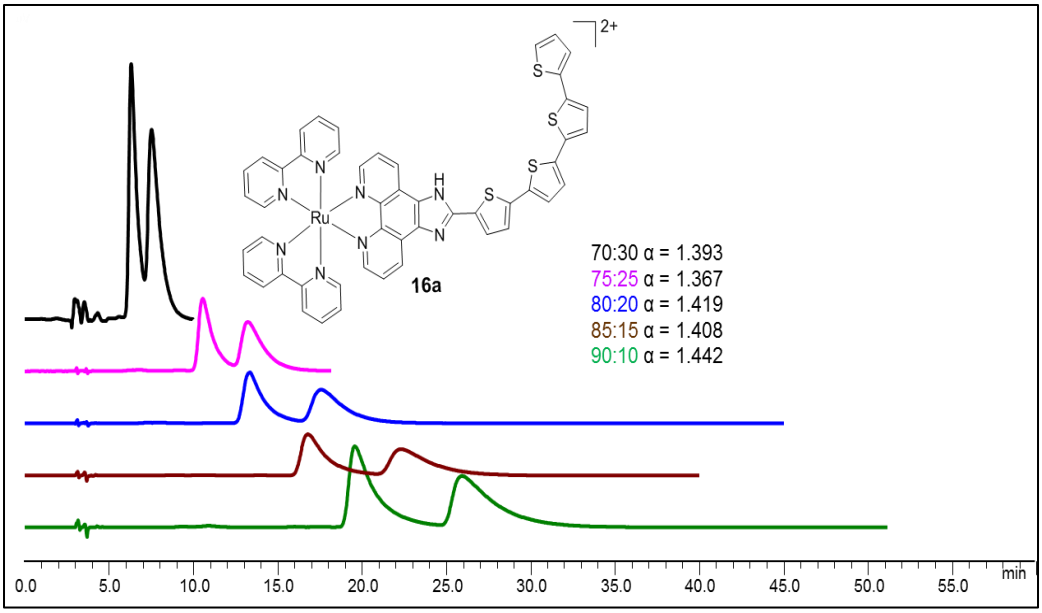

Figure 3.14 [$Ru(bpy)_2(dppn)$] $(PF_6)_2$ optimization study

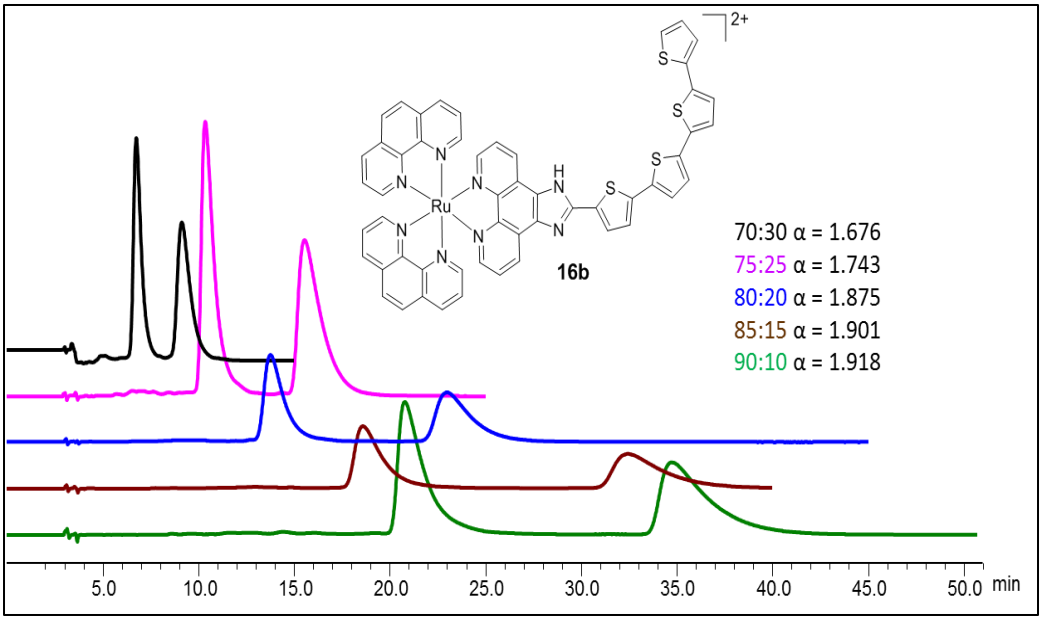

Figure 3.15 [Ru(phen)$_2$(ip-4t)] $(PF_6)_2$ optimization study

In summary, we found the optimal method for all of the Ru(II) complexes to 75:25 MeOH (with 0.025 M NH_4NO_3)/MeCN. However, the Ru(I) complex was found to be 80:20 MeOH (with 0.025 M NH_4NO_3)/MeCN. A summary of the results for all of the RPCs is seen in Table 3.1. As was seen with [Ru(phen)$_2$phendione] $(PF_6)_2$ resolution and selectivity remained relatively constant allowing the optimization to focus on retention time. From this data it will be possible to further develop a semi-preparative scale method for enantiopurification of the racemates for further analysis and testing.

Table 3.1 Summary of the results for method development of RPCs

$[Ru(bpy)_2(ip\text{-}4t)](PF_6)_2$ (16b)				
Mobile phase (with 0.025 M NH_4NO_3)	k_1	k_2	α	R_s
75 MeOH/25 MeCN	2.247	3.071	1.367	1.451
80 MeOH/20 MeCN	3.105	4.405	1.419	1.549
85 MeOH/15 MeCN	3.105	4.405	1.419	1.549
90 MeOH/10 MeCN	6.209	8.952	1.442	1.922

$[Ru(phen)_2(ip\text{-}4t)](PF_6)_2$ (16b)				
Mobile phase (with 0.025 M NH_4NO_3)	k_1	k_2	α	R_s
75 MeOH/25 MeCN	2.169	3.780	1.743	3.090
80 MeOH/20 MeCN	3.236	6.070	1.875	3.533
85 MeOH/15 MeCN	4.725	8.984	1.901	3.794
90 MeOH/10 MeCN	6.565	12.593	1.918	7.425

$[Ru(bpy)_2(dppn)](PF_6)_2$ (Rua2dppn)				
Mobile phase (with 0.025 M NH_4NO_3)	k_1	k_2	α	R_s
75 MeOH/25 MeCN	1.509	2.273	1.507	1.681
80 MeOH/20 MeCN	2.161	3.275	1.515	1.790
85 MeOH/15 MeCN	2.413	4.244	1.534	2.753
90 MeOH/10 MeCN	2.792	4.042	1.543	1.879

$[Ru(phen)_2(dppn)](PF_6)_2$ (Rub2dppn)				
Mobile phase (with 0.025 M NH_4NO_3)	k_1	k_2	α	R_s
75 MeOH/25 MeCN	1.356	2.891	2.132	3.838
80 MeOH/20 MeCN	1.973	4.165	2.111	4.237
85 MeOH/15 MeCN	2.918	6.092	2.088	4.346
90 MeOH/10 MeCN	3.893	7.568	2.130	4.477

$[Ru(phen)_2(ippy)](PF_6)_2$ (Rub2ippy)				
Mobile phase (with 0.025 M NH_4NO_3)	k_1	k_2	α	R_s
75 MeOH/25 MeCN	1.309	2.570	1.916	3.433
80 MeOH/20 MeCN	1.866	3.613	1.936	3.683
85 MeOH/15 MeCN	2.413	4.244	1.931	3.490
90 MeOH/10 MeCN	3.749	7.300	1.947	3.791

$[Ru(phen)_2(ip\text{-}4t)](PF_6)_2$ (Rua2pb16)				
Mobile phase (with 0.025 M NH_4NO_3)	k_1	k_2	α	R_s
75 MeOH/25 MeCN	1.393	1.598	1.147	2.516
80 MeOH/20 MeCN	1.665	1.914	1.149	1.685
85 MeOH/15 MeCN	2.089	2.440	1.168	1.804

References

1 Heron, M. P. D., Division of Vital Statistics In *National Vital Statistics Reports* 2013; Vol. 62.
2 Boulikas, T. *Anticancer Therapeutics*; Wiley-Blackwell A John Wiley & Sons, Ltd, 2008.
3 Elmore, S. *Toxicologic pathology* **2007**, *35*, 495.
4 Alibabaei, L.; Luo, H.; House, R. L.; Hoertz, P. G.; Lopez, R.; Meyer, T. J. *J. Mat. Chem. A* **2013**, *1*, 4133.
5 Zamble, D. B.; Lippard, S. J. *Trends in biochemical sciences* **1995**, *20*, 435.
6 Ishida, S.; Lee, J.; Thiele, D. J.; Herskowitz, I. *Proceedings of the National Academy of Sciences* **2002**, *99*, 14298.
7 Kristova, I. *Recent Patents on Anti-Cancer Drug Discovery* **2006**, *1*, 1.
8 Clarke, M. J. *Coord. Chem. Rev.* **2003**, *236*, 207.
9 Dwyer, F. P.; Goodwin, H. A.; Gyarfas, E. C. *Aust. J. Chem.* **1963**, *16*, 544.
10 Dwyer, F. P.; Gyarfas, E. C.; Rogers, W. P.; Koch, J. H. *Nature (London, U. K.)* **1952**, *170*, 190.
11 Dwyer FP, M. E., Roe EMF, Shulman A. *Br J Cancer* **1965**, *19*, 195.
12 Yadav, A.; Janaratne, T.; Krishnan, A.; Singhal, S. S.; Yadav, S.; Dayoub, A. S.; Hawkins, D. L.; Awasthi, S.; MacDonnell, F. M. *Mol. Cancer Ther.* **2013**, *12*, 643.
13 Gill, M. R.; Thomas, J. A. *Chem. Soc. Rev.* **2012**, *41*, 3179.
14 Gao, F.; Chao, H.; Wang, J.-Q.; Yuan, Y.-X.; Sun, B.; Wei, Y.-F.; Peng, B.; Ji, L.-N. *J. Biol. Inorg. Chem.* **2007**, *12*, 1015.
15 Shu, Y.; Breitbach, Z. S.; Dissanayake, M. K.; Perera, S.; Aslan, J. M.; Alatrash, N.; MacDonnell, F. M.; Armstrong, D. W. *Chirality* **2014**.
16 Inagaki, A.; Edure, S.; Yatsuda, S.; Akita, M. *Chemical Communications* **2005**, 5468.
17 Wang, C.; Ma, X.-X.; Li, J.; Xu, L.; Zhang, F.-x. *Journal of Molecular Catalysis A: Chemical* **2012**, *363-364*, 108.
18 Giribabu, L.; Bessho, T.; Srinivasu, M.; Vijaykumar, C.; Soujanya, Y.; Reddy, V. G.; Reddy, P. Y.; Yum, J.-H.; Grätzel, M.; Nazeeruddin, M. K. *Dalton Transactions* **2011**, *40*, 4497.
19 Banerjee, T.; Kaniyankandy, S.; Das, A.; Ghosh, H. N. *Inorganic Chemistry* **2013**, *52*, 5366.
20 Yu, Q.; Liu, Y.; Wang, C.; Sun, D.; Yang, X.; Liu, Y.; Liu, J. *PLoS ONE* **2012**, *7*, e50902.
21 Shi, S.; Liu, J.; Li, J.; Zheng, K. C.; Tan, C. P.; Chen, L. M.; Ji, L. N. *Dalton Transactions* **2005**, 2038.
22 Svensson, F. R.; Andersson, J.; Åmand, H. L.; Lincoln, P. *JBIC Journal of Biological Inorganic Chemistry* **2012**, *17*, 565.
23 Giorgio, F.; Edoardo, C.; Michela, P.; Daniele, Z.; Isabella, R. *European Journal of Inorganic Chemistry* **2012**, *2012*, 4365.

24 Lebwohl, D.; Canetta, R. *Eur. J. Cancer* **1998**, *34*, 1522.
25 Jung, Y.; Lippard, S. J. *Chem. Rev.* **2007**, *107*, 1387.
26 Farrell, N. *Comp. Coord. Chem. II* **2004**, *9*, 809.
27 Meng, X.; Leyva, M. L.; Jenny, M.; Gross, I.; Benosman, S.; Fricker, B.; et, a. *Cancer Res* **2009**, *69*, 5458.
28 Morris RE, A. R., Murdoch PdS, Chen H, Cummings J, Hughes ND, et al. *J Med Chem* **2001**, *44*, 3616.
29 Weiss, A.; Berndsen, R. H.; Dubois, M.; Muller, C.; Schibli, R.; Griffioen, A. W.; Dyson, P. J.; Nowak-Sliwinska, P. *Chem. Sci.* **2014**, *5*, 4742.
30 Graf, N.; Lippard, S. J. *Adv. Drug Deliv. Rev.* **2012**, *64*, 993.
31 Reisner, E.; Arion, V. B.; Keppler, B. K.; Pombeiro, A. J. L. *Inorganica Chimica Acta* **2008**, *361*, 1569.
32 Bergamo, A.; Gava, B.; Alessio, E.; Mestroni, G.; Serli, B.; Cocchietto, M.; Zorzet, S.; Sava, G. *Int. J. Oncol.* **2002**, *21*, 1331.
33 Depenbrock, H.; Schmelcher, S.; Peter, R.; Keppler, B.; Weirich, G.; Block, T.; Rastetter, J.; Hanauske, A.-R. *Eur. J. Cancer* **1997**, *33*, 2404.
34 Lentz, F.; Drescher, A.; Lindauer, A.; Henke, M.; Hilger, R. A.; Hartinger, C. G.; Scheulen, M. E.; Dittrich, C.; Keppler, B. K.; Jaehde, U. *Anti-cancer drugs* **2009**, *20*, 97.
35 Hartinger, C. G.; Jakupec, M. A.; Zorbas-Seifried, S.; Groessl, M.; Egger, A.; Berger, W.; Zorbas, H.; Dyson, P. J.; Keppler, B. K. *Chem. Biodivers.* **2008**, *5*, 2140.
36 Leijen, S.; Burgers, S. A.; Baas, P.; Pluim, D.; Tibben, M.; van Werkhoven, E.; Alessio, E.; Sava, G.; Beijnen, J. H.; Schellens, J. H. M. *Invest New Drugs* **2015**, *33*, 201.
37 Trondl, R.; Heffeter, P.; Kowol, C. R.; Jakupec, M. A.; Berger, W.; Keppler, B. K. *Chem. Sci.* **2014**, *5*, 2925.
38 Fong, J.; Kasimova, K.; Arenas, Y.; Kaspler, P.; Lazic, S.; Mandel, A.; Lilge, L. *Photochem. Photobiol. Sci.* **2015**, *14*, 2014.
39 Kaspler, P.; Lazic, S.; Forward, S.; Arenas, Y.; Mandel, A.; Lilge, L. *Photochem. Photobiol. Sci.* **2016**, *15*, 481.
40 Mari, C.; Pierroz, V.; Ferrari, S.; Gasser, G. *Chem. Sci.* **2015**, *6*, 2660.
41 Moucheron, C.; De Mesmaeker, A. K.; Kelly, J. M. *Struct. Bonding (Berlin)* **1998**, *92*, 163.
42 Swavey, S.; Brewer, K. J. *Inorg. Chem.* **2002**, *41*, 4044.
43 Sun, Y.; Joyce, L. E.; Dickson, N. M.; Turro, C. *Chem. Commun. (Cambridge, U. K.)* **2010**, *46*, 2426.
44 Lincoln, R.; Kohler, L.; Monro, S.; Yin, H.; Stephenson, M.; Zong, R.; Chouai, A.; Dorsey, C.; Hennigar, R.; Thummel, R. P.; McFarland, S. A. *J. Am. Chem. Soc.* **2013**, *135*, 17161.
45 Monro, S.; Scott, J.; Chouai, A.; Lincoln, R.; Zong, R.; Thummel, R. P.; McFarland, S. A. *Inorg. Chem.* **2010**, *49*, 2889.
46 Shi, G.; Monro, S.; Hennigar, R.; Colpitts, J.; Fong, J.; Kasimova, K.; Yin, H.; DeCoste, R.; Spencer, C.; Chamberlain, L.; Mandel, A.; Lilge, L.; McFarland, S. A. *Coord. Chem. Rev.* **2015**, *282-283*, 127.

47 Dickerson, M.; Sun, Y.; Howerton, B.; Glazer, E. C. *Inorg. Chem.* **2014**, *53*, 10370.
48 Ortmans, I.; Elias, B.; Kelly, J. M.; Moucheron, C.; Kirsch-DeMesmaeker, A. *Dalton. Trans.* **2004**, *4*, 668.
49 O'Reilly, F.; Kelly, J.; Mesmaeker, A. K.-D. *Chemical Commun.* **1996**, *9*, 1013.
50 Glazer, E. C. *Isr. J. Chem.* **2013**, *53*, 391.
51 Howerton, B. S.; Heidary, D. K.; Glazer, E. C. *J. Am. Chem. Soc.* **2012**, *134*, 8324.
52 Wachter, E.; Glazer, E. C. *J. Phys. Chem. A* **2014**, *118*, 10474.
53 Wachter, E.; Heidary, D. K.; Howerton, B. S.; Parkin, S.; Glazer, E. C. *Chem. Commun.* **2012**, *48*, 9649.
54 Dwyer, F. P.; Wright, R. D.; Shulman, A. *Austrailian Patent 251,582* **1964**, *[Chem Abstr., 66, 39465t (1967)]*, 24 pp.
55 White, D. O.; Harris, A. W.; Cheyne, I. M.; Shew, M. *Austral. J. Exp. Biol. Med. Sci.* **1969**, *47*, 81.
56 Schatzschneider, U.; Niesel, J.; Ott, I.; Gust, R.; Alborzinia, H.; Wölfl, S. *ChemMedChem* **2008**, *3*, 1104.
57 Dwyer, F. P.; Mayhew, E.; Roe, E. M. F.; Shulman, A. *Br. J. Cancer* **1965**, *19*, 195.
58 Koch JH, R. W., Dwyer FP, Gyarfas EC *Aust J Biol Sci* **1957**, *10*, 342.
59 Friedman, A. E.; Chambron, J. C.; Sauvage, J. P.; Turro, N. J.; Barton, J. K. *J. Am. Chem. Soc.* **1990**, *112*, 4960.
60 Liu, Y.; Chouai, A.; Degtyareva, N. N.; Lutterman, D. A.; Dunbar, K. R.; Turro, C. *J. Am. Chem. Soc.* **2005**, *127*, 10796.
61 Gill, M. R.; Derrat, H.; Smythe, C. G. W.; Battaglia, G.; Thomas, J. A. *ChemBioChem* **2011**, *12*, 877.
62 Augustyn, K. E.; Pierre, V. C.; K. Barton, J.; Begley, T. P. In *Wiley Encyclopedia of Chemical Biology*; John Wiley & Sons, Inc.: 2007.
63 Baggaley, E.; Gill, M. R.; Green, N. H.; Turton, D.; Sazanovich, I. V.; Botchway, S. W.; Smythe, C.; Haycock, J. W.; Weinstein, J. A.; Thomas, J. A. *Angew. Chem., Int. Ed.* **2014**, *53*, 3367.
64 Gill, M. R.; Cecchin, D.; Walker, M. G.; Mulla, R. S.; Battaglia, G.; Smythe, C.; Thomas, J. A. *Chem. Sci.* **2013**, *4*, 4512.
65 Gill, M. R.; Garcia-Lara, J.; Foster, S. J.; Smythe, C.; Battaglia, G.; Thomas, J. A. *Nat Chem* **2009**, *1*, 662.
66 Meggers, E. *Curr Opin Chem Biol* **2007**, *11*, 287.
67 Pisani MJ, W. D., Heimann K, Collins JG, Keene FR. *Metallomics* **2010**, *2*, 393.
68 Pascu, G. I.; Hotze, A. C.; Sanchez-Cano, C.; Kariuki, B. M.; Hannon, M. J. *Angewandte Chemie (International ed. in English)* **2007**, *46*, 4374.
69 Spillane, C. B.; Fletcher, N. C.; Rountree, S. M.; Berg, H.; Chanduloy, S.; Morgan, J. L.; Keene, F. R. *J. Biol. Inorg. Chem.* **2007**, *16*, 797.
70 Velders, A. H.; Kooijman, H.; Spek, A. L.; Haasnoot, J. G.; De Vos, D.; Reedijk, J. *Inorg. Chem.* **2000**, *39*, 2966.

71 McDonnell, U.; Kerchoffs, J. M. C. A.; Castineiras, R. P. M.; Hicks, M. R.; Hotze, A. C. G.; Hannon, M. J.; Rodger, A. *Dalton Trans.* **2008**, 667.
72 Novakova, O.; Kasparkova, J.; Vrana, O.; van Vliet, P. M.; Reedijk, J.; Brabec, V. *Biochemistry* **1995**, *34*, 12369.
73 Tan, C.; Lai, S.; Wu, S.; Hu, S.; Zhou, L.; Chen, Y.; Wang, M.; Zhu, Y.; Lian, W.; Peng, W. *J. Med. Chem.* **2010**, *53*, 7613.
74 Gill, M. R.; Harun, S. N.; Halder, S.; Boghozian, R. A.; Ramadan, K.; Ahmad, H.; Vallis, K. A. *Sci. Rep.* **2016**, *6*.
75 Zeng, L.; Chen, Y.; Liu, J.; Huang, H.; Guan, R.; Ji, L.; Chao, H. *Sci. Rep.* **2016**, *6*, 19449.
76 Foxon, S. P.; Phillips, T.; Gill, M. R.; Towrie, M.; Parker, A. W.; Webb, M.; Thomas, J. A. *Angew. Chem. Int. Ed.* **2007**, *46*, 3686.
77 Puckett, C. A.; Barton, J. K. *Bioorg. Med. Chem.* **2010**, *18*, 3564.
78 Brabec V, N. O. *Drug Resist Updates* **2006**, *9*, 111.
79 Pisani, M. J.; Fromm, P. D.; Mulyana, Y.; Clarke, R. J.; Körner, H.; Heimann, K.; Collins, J. G.; Keene, F. R. *ChemMedChem* **2011**, *6*, 848.
80 Pierroz, V.; Joshi, T.; Leonidova, A.; Mari, C.; Schur, J.; Ott, I.; Spiccia, L.; Ferrari, S.; Gasser, G. *J. Am. Chem. Soc.* **2014**, *134*, 20376.
81 Tan, C.; Wu, S.; Lai, S.; Wang, M.; Chen, Y.; Zhou, L.; Zhu, Y.; Lian, W.; Peng, W.; Ji, L.; Xu, A. *Dalton Trans.* **2011**, *40*, 8611.
82 Puckett, C. A.; Barton, J. K. *J. Am. Chem. Soc.* **2007**, *129*, 46.
83 Puckett, C. A.; Barton, J. K. *Biochemistry* **2008**, *47*, 11711.
84 Du, Y.; Fu, X.; Li, H.; Chen, B.; Guo, Y.; Su, G.; Zhang, H.; Ning, F.; Lin, Y.; Mei, W.; Chen, T. *ChemMedChem* **2014**, *9*, 714.
85 Li, F.; Harry, E. J.; Bottomley, A. L.; Edstein, M. D.; Birrell, G. W.; Woodward, C. E.; Keene, F. R.; Collins, J. G. *Chem. Sci.* **2014**, *5*, 685.
86 Schatzschneider U, N. J., Ott I, Gust R, Alborzinia H, Wölfl S. *ChemMedChem* **2008**, *3*, 1104.
87 Liu, Y.-J.; Zeng, C.-H.; Liang, Z.-H.; Yao, J.-H.; Huang, H.-L.; Li, Z.-Z.; Wu, F.-H. *Eur. J. Med. Chem.* **2010**, *45*, 3087.
88 Joshi, T.; Pierroz, V.; Mari, C.; Gemperle, L.; Ferrari, S.; Gasser, G. *Angew. Chem. Int. Ed.* **2014**, *53*, 2960.
89 Vos, J. G.; Kelly, J. M. *Dalton Trans.* **2006**, 4869.
90 Janaratne, T. K.; Yadav, A.; Ongeri, F.; MacDonnell, F. M. *Inorg. Chem.* **2007**, *46*, 3420.
91 Sun Y, J. L., Dickson NM, Turro C *Chem Commun* **2010**, *46*, 2426.
92 Joshi, T.; Pierroz, V.; Ferrari, S.; Gasser, G. *ChemMedChem* **2014**, *9*, 1419.
93 Kabingu, E.; Oseroff, A. R.; Wilding, G. E.; Gollnick, S. O. *Clin. Cancer Res.* **2009**, *15*, 4460.
94 Burstall, F. H. *J. Chem. Soc.* **1936**, 173.
95 Mabrouk, P. A.; Wrighton, M. S. *Inorg. Chem.* **1986**, *25*, 526.
96 Wärnmark, K.; Heyke, O.; Thomas, J. A.; Lehn, J.-M. *Chem. Commun.* **1996**, 2603.

97 Kim, M.-J.; Konduri, R.; Ye, H.; MacDonnell, F. M.; Puntoriero, F.; Serroni, S.; Campagna, S.; Holder, T.; Kinsel, G.; Rajeshwar, K. *Inorg. Chem.* **2002**, *41*, 2471.
98 MacDonnell, F. M.; Bodige, S. *Inorg. Chem.* **1996**, *35*, 5758.
99 Bolger, J.; Gourdon, A.; Ishow, E.; Launay, J.-P. *Inorg. Chem.* **1996**, *35*, 2937.
100 Crey, C.; Dumy, P.; Lhomme, J.; Kotera, M. *Synth Commun* **2003**, *33*, 3727.
101 Goyne, T. E.; Sigman, D. S. *J. Am. Chem. Soc.* **1987**, *9*, 2846.
102 Krumova, K.; Cosa, G. In *Photochemistry: Volume 41*; The Royal Society of Chemistry: 2013; Vol. 41, p 279.
103 Metcalfe, C.; Thomas, J. A. *Chem. Soc. Rev.* **2003**, *32*, 215.
104 Le, V. H.; McGuire, M. R.; Ahuja, P.; MacDonnell, F. M.; Lewis, E. A. *J. Phys. Chem. A.* **2015**, *119*, 65.
105 Balzani, V.; Juris, A.; Venturi, M.; Campagna, S.; Serroni, S. *Chem. Rev.* **1996**, *96*, 759.
106 Schafer, F. Q.; Buettner, G. R. *Free Radic. Biol. Med.* **2001**, *30*, 1191.
107 Sinha, B. K.; Politi, P. M. *Cancer. Chemother. Biol. Response Modif.* **1990**, *11*, 45.
108 Gewirtz, D. A. *Biochem. Pharmacol.* **1999**, *57*, 727.
109 Wondrak, G. T. *Antioxid. Redox Signal.* **2009**, *11*, 3013.
110 Oroskar, A. A.; Lambert, C.; Peak, M. J. *Free Radic. Biol. Med.* **1996**, *20*, 751.
111 Bates, D. A.; Winterbourn, C. C. *FEBS Lett.* **1982**, *145*, 137.
112 Pogozelski, W. K.; Tullius, T. D. *Chem. Rev.* **1998**, *98*, 1089.
113 Sonntag, C. v. *Free-radical-induced DNA damage and its repair: a chemical perspective*; 1 ed.; Springer-Verlag Berlin Heidelberg: New York, Berlin, 2006.
114 Giandomenico, A. R.; Cerniglia, G. E.; Biaglow, J. E.; Stevens, C. W.; Koch, C. J. *Free Radic. Biol. Med.* **1997**, *23*, 426.
115 Franco, R.; Panayiotidis, M. I.; Cidlowski, J. A. *The Journal of biological chemistry* **2007**, *282*, 30452.
116 Kang, P.; Chen, Z.; Nayak, A.; Zhang, S.; Meyer, T. J. *Energy & Environmental Science* **2014**, *7*, 4007.
117 Aitken, C. E.; Marshall, R. A.; Puglisi, J. D. *Biophys. J.* **2008**, *94*, 1826.
118 Konduri, R.; MacDonnell, F. M.; Ye, H.; Rajeshwar, K.; Serroni, S.; Campagna, S.; American Chemical Society: 2002, p INOR.
119 Campos-Martin, J. M.; Blanco-Brieva, G.; Fierro, J. L. G. *Angew. Chem. Int. Ed.* **2006**, *45*, 6962.
120 James, T. H.; Snell, J. M.; Welsaberger, A. *J. Am. Chem. Soc.* **1938**, *60*, 2084.
121 Akagawa, M.; Shigemitsu, T.; Suyama, K. *Biosci. Biotechnol. Biochem.* **2003**, *67*, 2632.
122 Eberlein, G.; Bruice, T. C. *J. Am. Chem. Soc.* **1982**, *104*, 1449.
123 Kemal, C.; Chan, T. W.; Bruice, T. C. *J. Am. Chem. Soc.* **1977**, *99*, 7272.

124 Kashige, N.; Takeuchi, T.; Matsumoto, S.; Takechi, S.; Miake, F.; Yamaguchi, T. *Biol. Pharm. Bull.* **2005**, *28*, 419.
125 Goldstein, S.; Meyerstein, D.; Czapski, G. *Free Radic. Biol. Med.* **1993**, *15*, 435.
126 Burkitt, M. J.; Mason, R. P. *Proc. Natl. Acad. Sci. U.S.A.* **1991**, *88*, 8440.
127 Schreiber, J.; Mottley, C.; Sinha, B. K.; Kalyanaraman, B.; Mason, R. P. *J. Am. Chem. Soc.* **1987**, *109*, 348.
128 Kalyanaraman, B.; Morehouse, K. M.; Mason, R. P. *Arch Biochem Biophys* **1991**, *286*, 164.
129 Shah, P. K.; Bhattacharjee, K.; Shukla, P. K. *RSC Advances* **2016**, *6*, 113620.
130 Bergamo, A.; Gaiddon, C.; Schellens, J. H.; Beijnen, J. H.; Sava, G. *Journal of inorganic biochemistry* **2012**, *106*, 90.
131 Wu, J.; Chen, W.; Yin, Y.; Zheng, Z.; Zou, G. *Biometals : an international journal on the role of metal ions in biology, biochemistry, and medicine* **2014**, *27*, 445.
132 Burger, R. M. *Chemical Reviews* **1998**, *98*, 1153.
133 Chen, J.; Ghorai, M. K.; Kenney, G.; Stubbe, J. *Nucleic Acids Res* **2008**, *36*, 3781.
134 Mohler, D. L.; Downs, J. R.; Hurley-Predecki, A. L.; Sallman, J. R.; Gannett, P. M.; Shi, X. *J. Org. Chem.* **2005**, *70*, 9093.
135 Connolly, T. J.; Baldový´, M. V.; Mohtath, N.; Scaiano, J. C. *Tetrahedron Lett.* **1996**, *37*, 4919.
136 Brayton, C. F. *Cornell Vet* **1986**, *76*, 61.
137 Konduri, R.; de Tacconi, N. R.; Rajeshwar, K.; MacDonnell, F. M. *J Am Chem Soc* **2004**, *126*, 11621.
138 de Tacconi, N. R.; Lezna, R. O.; Konduri, R.; Ongeri, F.; Rajeshwar, K.; MacDonnell, F. M. *Chem. Eur. J.* **2005**, *11*, 4327.
139 Wellington, K. W. *RSC Adv* **2015**, *5*, 20309.
140 Yamaguchi, T.; Eto, M.; Harano, K.; Kashige, N.; Watanabe, K.; Ito, S. *Tetrahedron* **1999**, *55*, 675.
141 Yamaguchi, T.; Kashige, N.; Mishiro, N.; Miake, F.; Watanabe, K. *Biol. Pharm. Bull.* **1996**, *19*, 1261.
142 Yamaguchi, T.; Matsumoto, S.; Watanabe, K. *Tetrahedron Lett.* **1998**, *39*, 8311.
143 Mibu, N.; Yukawa, M.; Kashige, N.; Iwase, Y.; Goro, Y.; Miake, F.; Yamaguchi, T.; Ito, S.; Sumoto, K. *Chem. Pharm. Bull.* **2003**, *51*, 27.
144 Aranda, A.; Sequedo, L.; Tolosa, L.; Quintas, G.; Burello, E.; Castell, J. V.; Gombau, L. *Toxicol In Vitro* **2013**, *27*, 954.
145 Krumova, K.; Cosa, G. In *Singlet Oxygen: Applications in Biosciences and Nanosciences, Volume 1*; The Royal Society of Chemistry: 2016; Vol. 1, p 1.
146 Bhat, T. A.; Kumar, S.; Chaudhary, A. K.; Yadav, N.; Chandra, D. *Drug Discov Today* **2015**, *20*, 635.

147 Qian, C.; Wang, J.-Q.; Song, C.-L.; Wang, L.-L.; Ji, L.-N.; Chao, H. *Metallomics* **2013**, *5*, 844.
148 Hergueta-Bravo, A.; Jimenez-Hernandez, M. E.; Montero, F.; Oliveros, E.; Orellana, G. *J. Phys. Chem. B.* **2002**, *106*, 4010.
149 Marechal, A.; Zou, L. *Cold Spring Harbor perspectives in biology* **2013**, *5*.
150 Tanaka, T.; Halicka, H. D.; Traganos, F.; Seiter, K.; Darzynkiewicz, Z. *Cell cycle (Georgetown, Tex.)* **2007**, *6*, 371.
151 Chou, W. C.; Hu, L. Y.; Hsiung, C. N.; Shen, C. Y. *Carcinogenesis* **2015**, *36*, 832.
152 Gamper, A. M.; Rofougaran, R.; Watkins, S. C.; Greenberger, J. S.; Beumer, J. H.; Bakkenist, C. J. *Nucleic Acids Res* **2013**, *41*, 10334.
153 Rogakou, E. P.; Pilch, D. R.; Orr, A. H.; Ivanova, V. S.; Bonner, W. M. *The Journal of biological chemistry* **1998**, *273*, 5858.
154 Tommasino, F.; Friedrich, T.; Jakob, B.; Meyer, B.; Durante, M.; Scholz, M. *PLoS One* **2015**, *10*, e0129416.
155 Burma, S.; Chen, B. P.; Murphy, M.; Kurimasa, A.; Chen, D. J. *The Journal of biological chemistry* **2001**, *276*, 42462.
156 Banath, J. P.; Macphail, S. H.; Olive, P. L. *Cancer Res* **2004**, *64*, 7144.
157 Banath, J. P.; Klokov, D.; MacPhail, S. H.; Banuelos, C. A.; Olive, P. L. *BMC cancer* **2010**, *10*, 4.
158 Redon, C.; Pilch, D.; Rogakou, E.; Sedelnikova, O.; Newrock, K.; Bonner, W. *Current opinion in genetics & development* **2002**, *12*, 162.
159 Banáth, J. P.; Klokov, D.; MacPhail, S. H.; Banuelos, C. A.; Olive, P. L. *BMC cancer* **2010**, *10*, 1.
160 Bonner, W. M.; Redon, C. E.; Dickey, J. S.; Nakamura, A. J.; Sedelnikova, O. A.; Solier, S.; Pommier, Y. *Nat Rev Cancer* **2008**, *8*, 957.
161 Ledesma-Fernández, E.; Thorpe, P. H. *J Biol Methods* **2015**, *2*, 62.
162 Teicher, B. A. *Cancer metastasis reviews* **1994**, *13*, 139.
163 Teicher, B. A.; Holden, S. A.; al-Achi, A.; Herman, T. S. *Cancer Res* **1990**, *50*, 3339.
164 Bard, A. J.; Faulkner, L. R. *Electrochemical Methods*; Wiley: New York, 1980.
165 Meyer, T. J. *Acc. Chem. Res.* **1989**, *22*, 163.
166 Sun, Y.; Liu, Y.; Turro, C. *Journal of the American Chemical Society* **2010**, *132*, 5594.
167 Singh, S.; de, T. N. R.; Boston, D.; MacDonnell, F. M. *Dalton Trans.* **2010**, *39*, 11180.
168 Barigelletti, F.; Juris, A.; Balzani, V.; Belser, P.; Von Zelewsky, A. *Inorganic Chemistry Communications* **1987**, *26*, 4115.
169 de Tacconi, N. R.; Lezna, R. O.; Chitakunye, R.; MacDonnell, F. M. *Inorg. Chem.* **2008**, *47*, 8847.
170 Boisdenghien, A.; Moucheron, C.; Kirsch-De Mesmaeker, A. *Inorg. Chem.* **2005**, *44*, 7678
171 Troian-Gautier, L.; Moucheron, C. *Molecules* **2014**, *19*, 5028.

172 Campagna, S.; Serroni, S.; Bodige, S.; MacDonnell, F. M. *Inorg. Chem.* **1999**, *38*, 692.
173 Fernandes, C.; Tiritan, E. M.; Pinto, M. M. *Symmetry* **2017**, *9*.
174 Brooks, W. H.; Guida, W. C.; Daniel, K. G. *Current topics in medicinal chemistry* **2011**, *11*, 760.
175 Armstrong, D. W.; DeMond, W.; Czech, B. P. *Anal. Chem.* **1985**, *57*, 481.
176 Chunxia, J.; Man-Yung, T.; W., A. D.; Sirantha, P.; Ye, B.; M., M. F. *Chirality* **2009**, *21*, 208.
177 Sun, P.; Krishnan, A.; Yadav, A.; MacDonnell, F. M.; Armstrong, D. W. *J. Mol. Struc.* **2008**, *890*, 75.
178 Sun, P.; Krishnan, A.; Yadav, A.; Singh, S.; MacDonnell, F. M.; Armstrong, D. W. *Inorg. Chem. (Washington, DC, U. S.)* **2007**, *46*, 10312.
179 Shu, Y.; Breitbach, Z. S.; Dissanayake, M. K.; Perera, S.; Aslan, J. M.; Alatrash, N.; MacDonnell, F. M.; Armstrong, D. W. *Chirality* **2015**, *27*, 64.
180 Kalíková, K.; Janečková, L.; Armstrong, D. W.; Tesařová, E. *Journal of Chromatography A* **2011**, *1218*, 1393.
181 Hartshorn, R. M.; Barton, J. K. *Journal of the American Chemical Society* **1992**, *114*, 5919.
182 Stephenson, M.; Reichardt, C.; Pinto, M.; Wächtler, M.; Sainuddin, T.; Shi, G.; Yin, H.; Monro, S.; Sampson, E.; Dietzek, B.; McFarland, S. A. *The Journal of Physical Chemistry A* **2014**, *118*, 10507.
183 Sainuddin, T.; McCain, J.; Pinto, M.; Yin, H.; Gibson, J.; Hetu, M.; McFarland, S. A. *Inorganic Chemistry* **2016**, *55*, 83.
184 McFarland, S. A.; A61P 35/00 (2006.01) ,C07F 19/00 (2006.01) ed.; Organization, W. I. P., Ed.; MCFARLAND SHERRI ANN: 2016.